IEEE Access
Multidisciplinary | Rapid Review | Open Access Journal

Received October 8, 2019, accepted October 20, 2019, date of publication October 24, 2019, date of current version November 6, 2019.

Digital Object Identifier 10.1109/ACCESS.2019.2949285

Robust Control Allocation in Attitude Fault-Tolerant Control for Combined Spacecraft Under Measurement Uncertainty

XIU-WEI HUANG[1] AND GUANG-REN DUAN[1,2], (Fellow, IEEE)
[1]Center for Control Theory and Guidance Technology, Harbin Institute of Technology, Harbin 150080, China
[2]State Key Laboratory of Robotics and System, Harbin Institute of Technology, Harbin 150080, China

Corresponding author: Guang-Ren Duan (g.r.duan@hit.edu.cn)

This work was supported in part by the Major Program of National Natural Science Foundation of China under Grant 61690210 and Grant 61690212, in part by the Self-Planned Task, State Key Laboratory of Robotics and System (HIT), under Grant SKLRS201716A, and in part by the National Natural Science Foundation of China under Grant 61333003.

ABSTRACT Attitude control of combined service-target system in the post-capture phase has received great attention. A new attitude dynamics of the combined spacecraft with reaction wheels has been established in the author's former work, however, the measurement uncertainty in attitude and angular velocity and uncertainty in the reconfiguration matrix of reaction wheels have not been considered, which may cause huge impact on the system performance. In this paper, a novel combination of disturbance-observer-based dynamic surface control under measurement uncertainty and robust control allocation due to uncertain mass center is investigated for attitude stabilization of the combined spacecraft. Firstly, considering measurement uncertainty, inertia uncertainty, actuator fault and actuator saturation, a new attitude dynamics of combined spacecraft is established. Then, a virtual controller is designed and all the states in the closed-loop system converge to a small neighborhood of zero, where the lumped disturbance is compensated by two stable nonlinear disturbance observers and adverse effect of actuator saturation is addressed by a stable compensator. Finally, in consideration of uncertain location of mass center in the reconfiguration matrix, a LMI-based robust control allocation is employed to deal with the problem of distributing the three axis torques over the reaction wheels. Numerical simulations are presented to illustrate the effectiveness of the proposed method.

INDEX TERMS Attitude control, dynamic surface, fault-tolerant control, measurement uncertainty, robust control allocation, combined spacecraft.

I. INTRODUCTION

In recent years, on-orbit failures have exceeded launch failures and cumulatively account for losses of billions of dollars [1]. In order to remove or extend operational lifetime of these failed spacecrafts, a service spacecraft installed with a robotic arm to capture them is an effective way.

Once the target is captured, the dynamics of the combined spacecraft will vary greatly due to the increase in mass and variation in the centre-of-mass [2]. In addition, the configuration matrix of reaction wheels suffering a large change will also influence the new attitude dynamics. A new attitude dynamic model of the combined spacecraft, considering the new configuration matrix of reaction wheels, has been determined in the new body frame of the combined system in [3]. However, since the attitude and angular velocity cannot be accurately derived by the measurement devices due to uncertain mass center of combined spacecraft and limitation in physical sensors, the measurement uncertainty is also needed to be considered in the new attitude dynamics of combined spacecraft [4]–[7]. Besides, actuator faults and actuator saturation are both critical issues that need to be tackled in attitude control design of combined spacecraft for performance degradation and physical limitation. In this paper, a novel attitude dynamics of combined spacecraft with rebuilt configuration matrix of reaction wheels considering measurement uncertainty, inertia uncertainty, actuator fault and actuator saturation is established.

The associate editor coordinating the review of this manuscript and approving it for publication was Huiping Li.

During the attitude dynamics rebuilding process, it will be noticed that the reconfiguration matrix of reaction wheels depends on the center-to-center distance vector from the body frame center of service spacecraft to the body frame of combined spacecraft. Since there is an estimation error in the body frame center of the combined spacecraft, the center-to-center distance vector will also suffer some estimation error. Therefore, a robust control allocation is required that maps an 'ideal' virtual control to each reaction wheel effectively even in the presence of this potentially significant uncertainty. In [8], Durham first investigated the control allocation problem, where body-axis moments were allocated to several airplane flight controls. Then several approaches of control allocation have been deeply investigated in the last decade, including direct allocation [9], linear or nonlinear programming based on optimization algorithms [10], and dynamic control allocation [11], [12]. In reality, due to finite manufacturing tolerances or warping of the spacecraft structure during launch [13], the configuration matrix always exists some uncertainty, robust control allocation problems were then widely studied. In [14] and [15], a robust control allocation (RobCA) strategy, formulated as a min-max nonlinear optimization problem, was proposed to redistribute a virtual control signal to the remaining actuators when actuator fault occurred. Different from the above nonlinear programming problem, in this paper, the robust control allocation problem is formulated as a LMI-based linear programming problem, which immensely reduces the complexity of computation comparing to the existing methods.

As the input to the RobCA, the 'virtual' control torque for high-standard attitude control of combined spacecraft is also one challenging operation need to be settled. For the uncertainty in the mass center of the combined spacecraft, there exists some uncertainty in the inertia matrix. A robust nonlinear controller for the tethered space robot-target combination was proposed based on the backstepping control method in [16], [17]. Actuator saturation is a critical issue that needs to be tackled in attitude control design of combined spacecraft for the limitation of the physical characteristics [18], [19]. The most prominent method among all the solutions for actuator saturation is the anti-windup design [20], [21]. The occurrence of actuator faults may lead to performance degradation or instability of the closed-loop system, which should also be considered in the attitude stabilization control of combined spacecraft. In [22] and [23], adaptive non-linear fault estimation observer was designed to obtain the estimated value of unknown actuator faults. In [24], the problem of adaptive fault estimation and accommodation for a class of stochastic nonlinear systems with unknown time-varying faults was studied. Besides inertia uncertainty, actuator saturation and actuator fault, the accurate attitude and angular velocity may not be precisely derived by the measurement devices for roughly disturbed environmental condition. Thus the measurement uncertainty is also involved in the attitude controller design of combined spacecraft. In paper [25] and [26], the attitude control problem with measurement error was investigated, and a noise reduction extended disturbance observer and a finite-time integral sliding mode disturbance observer were used to estimate the integrated uncertainties, respectively. In this paper, two disturbance-observers-based dynamic surface control method is used to develop the virtual attitude control. Comparing to existing method, there is only one adjusting parameter in each observer, where the complexity of computation is reduced. And also the 'explosion of complexity' of the backstepping method is restrained by the dynamic method [27].

In this paper, we provide a robust fault-tolerant control strategy for rebuilt attitude control system of combined spacecraft with reaction wheels in the presence of inertia uncertainty, actuator saturation, and even measurement uncertainty. This proposed control law is a combination of disturbance-observer-based dynamic surface control and robust LMI-based control allocation. The main contributions of this paper are stated as follows:

1. The new attitude dynamics of the combined spacecraft system with reconfiguration matrix of reaction wheels considering inertia uncertainty, actuator saturation, actuator fault and measurement uncertainty is established.

2. A virtual controller based on two nonlinear simple disturbance observers and dynamic surface control is developed which ensures all the states in the closed-loop system converge to a small neighborhood of zero.

3. A novel LMI-based RobCA scheme is proposed considering the actuator saturation and the uncertainties in the reconfiguration matrix induced by post-capture of the target.

This paper is organized as follows: section II establishes the attitude dynamic equation of combined spacecraft with reaction wheels under inertia uncertainties, measurement uncertainties, actuator fault and actuator saturation. In section III, two nonlinear disturbance observers based dynamic surface control scheme is developed to produce virtual control torque, and a LMI-based robust control allocation is developed to distribute the virtual control torque into each reaction wheel. Finally, section IV presents numerical simulations for the combined spacecraft attitude system which illustrate the effectiveness of the proposed approach.

II. PROBLEM DESCRIPTION

In this paper, in order to form the attitude stabilization control system of the combined spacecraft, several corresponding frames are defined. The orbit frame $\mathcal{F}_o(O_c x_o y_o z_o)$ defines the centroid of combined spacecraft as its origin, the $O_c x_o$ axis is along the local horizontal direction in the orbital plane, the $O_c y_o$ axis is along the orbital normal and the $O_c z_o$ axis is collinear with a line that extends from the center of the earth to the centroid of combined spacecraft and completes a right-handed triad. Similarly, $\mathcal{F}_c(O_c x_c y_c z_c)$, $\mathcal{F}_s(O_s x_s y_s z_s)$ and $\mathcal{F}_t(O_t x_t y_t z_t)$ denote the body frame of combined spacecraft, the body frame of service spacecraft and the body frame of target spacecraft, respectively.

We also assume that the combined spacecraft system consists of a rigid service spacecraft, a rigid target spacecraft

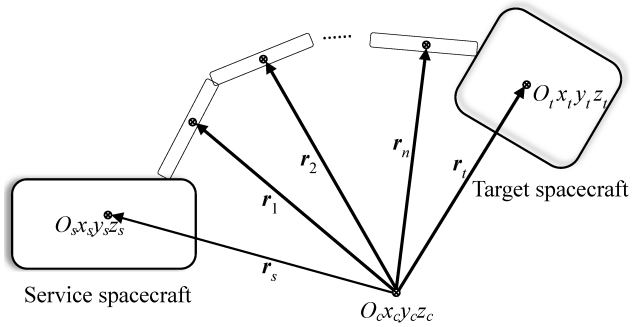

FIGURE 1. Model of space manipulators robot on service spacecraft.

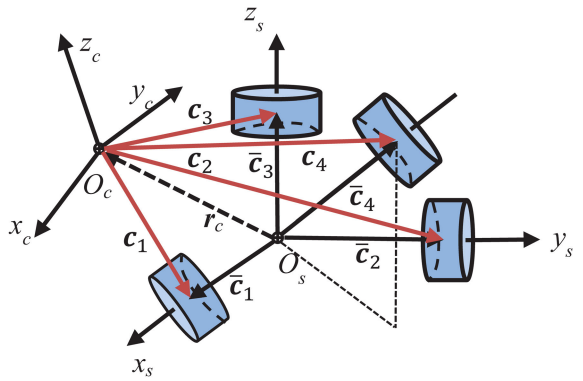

FIGURE 2. Reaction wheels configuration before and after capturing target spacecraft.

and one rigid space manipulator. The launch vehicle interface ring of target spacecraft is captured by the space manipulator, shown in the Fig. 1. In the post-capture phase, the joints of space manipulators would be locked.

For the simpleness of statement, similar to [28], the following assumptions need to be satisfied:

Assumption 1: There is no attitude control capability in the target spacecraft, whose attitude control is taken over by the attitude control system of the service spacecraft.

Assumption 2: The service spacecraft is driven by reaction wheels which are assumed to be continuously controllable.

Assumption 3: Once the joints of the space manipulators are locked, the space manipulators are locked.

Based on Assumption 3, the combined spacecraft can be seen as a rigid body in the post-capture phase. For the inertia matrix of the combined spacecraft in $\mathcal{F}_c(O_c x_c y_c z_c)$, relevant result has been conducted in [2]. After simple derivation, we can obtain that the inertia matrix of combined spacecraft expressed in $\mathcal{F}_c(O_c x_c y_c z_c)$ can be computed as

$$\begin{aligned}\boldsymbol{J} &= \boldsymbol{R}_s \boldsymbol{J}_s \boldsymbol{R}_s^{\mathrm{T}} + m_s[(\boldsymbol{r}_s^{\mathrm{T}}\boldsymbol{r}_s)\boldsymbol{I}_3 - \boldsymbol{r}_s\boldsymbol{r}_s^{\mathrm{T}}] \\ &\quad + \sum_{i=1}^{n}(\boldsymbol{R}_i \boldsymbol{J}_i \boldsymbol{R}_i^{\mathrm{T}} + m_i[(\boldsymbol{r}_i^{\mathrm{T}}\boldsymbol{r}_i)\boldsymbol{I}_3 - \boldsymbol{r}_i\boldsymbol{r}_i^{\mathrm{T}}]) \\ &\quad + \boldsymbol{R}_t \boldsymbol{J}_t \boldsymbol{R}_t^{\mathrm{T}} + m_t[(\boldsymbol{r}_t^{\mathrm{T}}\boldsymbol{r}_t)\boldsymbol{I}_3 - \boldsymbol{r}_t\boldsymbol{r}_t^{\mathrm{T}}]\end{aligned}$$

where $\boldsymbol{I}_3$ denotes a 3×3 identity matrix; m_s, m_t, m_i $(i = 1, \cdots, n)$ are respectively the mass of service spacecraft and target spacecraft, and the i-th link of manipulator; $\boldsymbol{r}_s$, $\boldsymbol{R}_s$, $\boldsymbol{r}_t$ and $\boldsymbol{R}_t$ are respectively the centroid position vector, attitude rotation matrix of service spacecraft and target spacecraft; $\boldsymbol{J}_s, \boldsymbol{J}_t, \boldsymbol{J}_i$ $(i = 1, \cdots, n)$ are respectively the inertia tensor of service spacecraft, target spacecraft and the i-th link of manipulator; $\boldsymbol{r}_i$ and $\boldsymbol{R}_i$ $(i = 1, \cdots, n)$ are respectively the centroid position vector and attitude rotation matrix of the i-th link of manipulator.

In this paper, the MRP vector $\boldsymbol{\sigma} = \boldsymbol{e}\tan(\vartheta/4)$ with Euler's principal rotation axis $\boldsymbol{e}$ and angle ϑ is used to represent the spacecraft's attitude orientation, then the kinematics of the combined spacecraft is expressed as

$$\dot{\boldsymbol{\sigma}} = \boldsymbol{G}(\boldsymbol{\sigma})\boldsymbol{\omega} \tag{1}$$

where $\boldsymbol{\sigma} = [\sigma_1, \sigma_2, \sigma_3]^{\mathrm{T}}$ and $\boldsymbol{G}(\boldsymbol{\sigma})$ is the kinematics matrix expressed as

$$\boldsymbol{G}(\boldsymbol{\sigma}) = \frac{1}{4}\left[(1 - \boldsymbol{\sigma}^{\mathrm{T}}\boldsymbol{\sigma})\boldsymbol{I}_3 + 2\boldsymbol{\sigma}^{\times} + 2\boldsymbol{\sigma}\boldsymbol{\sigma}^{\mathrm{T}}\right]$$

where for any vector $\boldsymbol{z} = [z_1, z_2, z_3]^{\mathrm{T}} \in \mathbb{R}^3$, $\boldsymbol{z}^{\times}$ is defined as

$$\boldsymbol{z}^{\times} = \begin{bmatrix} 0 & -z_3 & z_2 \\ z_3 & 0 & -z_1 \\ -z_2 & z_1 & 0 \end{bmatrix}$$

Now let us consider the attitude dynamic of the combined spacecraft with reaction wheels in the body frame of combined spacecraft. The configuration of reaction wheels is described in Fig. 2 [3].

According to the result in [3], the angular momentum of the whole reaction wheels respect to the mass center of combined spacecraft O_c expressed in the frame $\mathcal{F}_c(O_c x_c y_c z_c)$ is denoted as

$$\boldsymbol{H}_w = \boldsymbol{C}\boldsymbol{h}_w \tag{2}$$

where $\boldsymbol{C}$ is the reaction wheels configuration matrix expressed in the frame $\mathcal{F}_c(O_c x_c y_c z_c)$, defined as

$$\boldsymbol{C} = \begin{bmatrix} \boldsymbol{c}_1 & \boldsymbol{c}_2 & \boldsymbol{c}_3 & \boldsymbol{c}_4 \end{bmatrix} \tag{3}$$

with $\boldsymbol{c}_i$ is the position vector of the i-th reaction wheel expressed in the frame $\mathcal{F}_c(O_c x_c y_c z_c)$ and can be written as

$$\boldsymbol{c}_i = \boldsymbol{R}_{sc}(\bar{\boldsymbol{c}}_i - \boldsymbol{r}_c) \tag{4}$$

where $\boldsymbol{R}_{sc}$ is the rotation matrix from frame $\mathcal{F}_s(O_s x_s y_s z_s)$ to $\mathcal{F}_c(O_c x_c y_c z_c)$, $\bar{\boldsymbol{c}}_i$ is the position vector of the i-th reaction wheel expressed in the frame $\mathcal{F}_s(O_s x_s y_s z_s)$ and $\boldsymbol{r}_c$ is the vector from O_s to O_c expressed in $\mathcal{F}_s(O_s x_s y_s z_s)$.

Due to measurement and computational errors when determine the location of the mass center of the combined chaser-target, there must be uncertainty in the position vector $\boldsymbol{r}_c$, where

$$\boldsymbol{r}_c = \boldsymbol{r}_{c0} + \Delta\boldsymbol{r}_c \tag{5}$$

with $\boldsymbol{r}_{c0} = [r_{c01}, r_{c02}, r_{c03}]^{\mathrm{T}}$ and measurement error $\Delta\boldsymbol{r}_c = [\Delta r_{c1}, \Delta r_{c2}, \Delta r_{c3}]^{\mathrm{T}}$, then the configuration matrix $\boldsymbol{C}$ can be denoted as

$$\boldsymbol{C} = \boldsymbol{C}_0 + \Delta\boldsymbol{C} \tag{6}$$

where

$$\boldsymbol{C}_0 = \boldsymbol{R}_{sc}\bar{\boldsymbol{C}} - \boldsymbol{R}_{sc}\boldsymbol{r}_{c0}\boldsymbol{e}_1^T, \tag{7}$$
$$\Delta\boldsymbol{C} = \boldsymbol{R}_{sc}\Delta\boldsymbol{r}_c\boldsymbol{e}_1^T \tag{8}$$

and

$$\boldsymbol{e}_1^T = \begin{bmatrix} 1 & 1 & 1 & 1 \end{bmatrix}$$

Now according to the above analysis, the total angular momentum $\boldsymbol{H}$ of combined spacecraft considering four reaction wheels mounted on the service spacecraft can be denoted by

$$\boldsymbol{H} = \boldsymbol{J}\boldsymbol{\omega} + \boldsymbol{H}_w = \boldsymbol{J}\boldsymbol{\omega} + (\boldsymbol{C}_0 + \Delta\boldsymbol{C})\boldsymbol{J}_w\boldsymbol{\Omega}_w \tag{9}$$

Then the dynamic system of the attitude control system expressed in the body frame of combined spacecraft $\mathcal{F}_c(O_c x_c y_c z_c)$ can be denoted as

$$\boldsymbol{J}\dot{\boldsymbol{\omega}} + (\boldsymbol{C}_0 + \Delta\boldsymbol{C})\boldsymbol{J}_w\dot{\boldsymbol{\Omega}}_w + \boldsymbol{\omega} \times \boldsymbol{H} = \boldsymbol{T}_{ext} \tag{10}$$

where $\boldsymbol{T}_{ext}$ is the total external torque imposing on the combined spacecraft. In this paper, the total external torque contains the gravity gradient torque $\boldsymbol{u}_g \in \mathbb{R}^3$ and the disturbance torque $\boldsymbol{d} \in \mathbb{R}^3$, i.e., $\boldsymbol{T}_{ext} = \boldsymbol{u}_g + \boldsymbol{d}$, then the dynamics and kinematics of the combined spacecraft expressed in the frame $\mathcal{F}_c(O_c x_c y_c z_c)$ can be rewritten as

$$\begin{cases} \dot{\boldsymbol{\sigma}} = \boldsymbol{G}(\boldsymbol{\sigma})\boldsymbol{\omega} \\ \boldsymbol{J}\dot{\boldsymbol{\omega}} = -\boldsymbol{\omega} \times (\boldsymbol{J}\boldsymbol{\omega} + (\boldsymbol{C}_0 + \Delta\boldsymbol{C})\boldsymbol{J}_w\boldsymbol{\Omega}_w) \\ -\boldsymbol{C}\boldsymbol{J}_w\dot{\boldsymbol{\Omega}}_w + \boldsymbol{u}_g + \boldsymbol{d} \end{cases} \tag{11}$$

To simplify matters, we shall restrict ourselves to the case of a circular Keplerian orbit. Then according to the analysis in Chapter 16.1 in [29], the gravity gradient torque $\boldsymbol{u}_g$ can be computed by

$$\boldsymbol{u}_g = 3\omega_0^2\boldsymbol{R}_3(\boldsymbol{\sigma}) \times \boldsymbol{J}\boldsymbol{R}_3(\boldsymbol{\sigma}) \tag{12}$$

where ω_0 is the orbit angular rate value and $\boldsymbol{R}_3(\boldsymbol{\sigma})$ can be expressed as

$$\boldsymbol{R}_3(\boldsymbol{\sigma}) = \frac{1}{(1 + \boldsymbol{\sigma}^{\mathrm{T}}\boldsymbol{\sigma})}\begin{bmatrix} 8\sigma_1\sigma_3 - 4\sigma_2(1 - \boldsymbol{\sigma}^{\mathrm{T}}\boldsymbol{\sigma}) \\ 8\sigma_2\sigma_3 + 4\sigma_1(1 - \boldsymbol{\sigma}^{\mathrm{T}}\boldsymbol{\sigma}) \\ 4(\sigma_3^2 - \sigma_2^2 - \sigma_1^2) + (1 - \boldsymbol{\sigma}^{\mathrm{T}}\boldsymbol{\sigma})^2 \end{bmatrix}$$

For better addressing the mismatched uncertainty on the control torque, with the idea of control allocation, we define the virtual control torque $\boldsymbol{u}$ as

$$\boldsymbol{u} = \boldsymbol{C}\boldsymbol{J}_w\dot{\boldsymbol{\Omega}}_w \tag{13}$$

Here, we assume that $\mathrm{rank}(\boldsymbol{C}\boldsymbol{J}_w) = 3$, which means that only full-actuated case is considered in this paper. Then, we can obtain the attitude kinematics and dynamics of combined spacecraft with reaction wheels under external disturbance as follows:

$$\begin{cases} \dot{\boldsymbol{\sigma}} = \boldsymbol{G}(\boldsymbol{\sigma})\boldsymbol{\omega} \\ \boldsymbol{J}\dot{\boldsymbol{\omega}} = -\boldsymbol{\omega}^{\times}(\boldsymbol{J}\boldsymbol{\omega} + (\boldsymbol{C}_0 + \Delta\boldsymbol{C})\boldsymbol{J}_w\boldsymbol{\Omega}_w) \\ -\boldsymbol{u} + \boldsymbol{u}_g + \boldsymbol{d} \end{cases} \tag{14}$$

A. MEASUREMENT UNCERTAINTY

Since the attitude and angular velocity are measured by many sensors mounted on the service spacecraft and the sensors are effected by complicated space environment, the measurement quantities are generally uncertain and can be expressed as [30]

$$\begin{cases} \hat{\boldsymbol{\sigma}} = \boldsymbol{\sigma} + \boldsymbol{\upsilon}_1 \\ \hat{\boldsymbol{\omega}} = \boldsymbol{\omega} + \boldsymbol{\upsilon}_2 \end{cases} \tag{15}$$

where $\boldsymbol{\upsilon}_1$ and $\boldsymbol{\upsilon}_2$ are the measurement uncertainties, which are both assumed to be differential. Furthermore, taking the time derivative of $\hat{\boldsymbol{\sigma}}$ and $\hat{\boldsymbol{\omega}}$ results in

$$\begin{cases} \dot{\hat{\boldsymbol{\sigma}}} = \boldsymbol{G}(\hat{\boldsymbol{\sigma}})\hat{\boldsymbol{\omega}} + \boldsymbol{\delta}_1 \\ \boldsymbol{J}\dot{\hat{\boldsymbol{\omega}}} = -\hat{\boldsymbol{\omega}}^{\times}(\boldsymbol{J}\hat{\boldsymbol{\omega}} + \boldsymbol{C}_0\boldsymbol{J}_w\boldsymbol{\Omega}) - \boldsymbol{u} + \boldsymbol{u}_g + \boldsymbol{\delta}_{20} \end{cases} \tag{16}$$

where

$$\begin{aligned} \boldsymbol{G}(\hat{\boldsymbol{\sigma}}) &= \frac{1}{4}[(1 - \hat{\boldsymbol{\sigma}}^{\mathrm{T}}\hat{\boldsymbol{\sigma}})\boldsymbol{I}_3 + 2\hat{\boldsymbol{\sigma}}^{\times} + 2\hat{\boldsymbol{\sigma}}\hat{\boldsymbol{\sigma}}^{\mathrm{T}}] \\ \boldsymbol{\delta}_1 &= \frac{1}{4}[(2\hat{\boldsymbol{\sigma}}^{\mathrm{T}}\boldsymbol{\upsilon}_1 - \boldsymbol{\upsilon}_1^{\mathrm{T}}\boldsymbol{\upsilon}_1)\boldsymbol{I}_3 - 2\boldsymbol{\upsilon}_1^{\times} - \hat{\boldsymbol{\sigma}}\boldsymbol{\upsilon}_1^{\mathrm{T}} - \boldsymbol{\upsilon}_1\hat{\boldsymbol{\sigma}}^T \\ &\quad + 2\boldsymbol{\upsilon}_1\boldsymbol{\upsilon}_1^{\mathrm{T}}]\hat{\boldsymbol{\omega}} - \boldsymbol{G}(\boldsymbol{\sigma})\boldsymbol{\upsilon}_2 + \dot{\boldsymbol{\upsilon}}_1 \\ \boldsymbol{\delta}_{20} &= -\hat{\boldsymbol{\omega}}^{\times}(-\boldsymbol{J}\boldsymbol{\upsilon}_2 + \Delta\boldsymbol{C}\boldsymbol{J}_w\boldsymbol{\Omega}_w) + \boldsymbol{\upsilon}_2^{\times}(\boldsymbol{J}(\hat{\boldsymbol{\omega}} - \boldsymbol{\upsilon}_2) \\ &\quad + \boldsymbol{C}\boldsymbol{J}_w\boldsymbol{\Omega}_w) + \boldsymbol{d} + \boldsymbol{J}\dot{\boldsymbol{\upsilon}}_2 \end{aligned}$$

Remark 1: The measurement uncertainty in $\boldsymbol{u}_g$ is reasonably ignored. Because the orbit angular rate $\omega_0 = 7.292115 \times 10^{-5}$ is very small, the value of $\boldsymbol{u}_g$ is also small, then the uncertainty caused by measurement uncertainty is far smaller comparing to the control torque produced by actuator.

B. INERTIA UNCERTAINTY

From the above analysis, it is hard to determine the mass center of combined spacecraft. Thus, the inertia matric of combined spacecraft cannot be precisely determined. To signify the error between true inertia matrix and estimated one of combined spacecraft, we set

$$\boldsymbol{J} = \boldsymbol{J}_0 + \Delta\boldsymbol{J} \tag{17}$$

where $\boldsymbol{J}_0$ denotes the estimated value of the inertia tensor of the combined spacecraft, $\Delta\boldsymbol{J}$ denotes the estimated error of the inertia tensor of the combined spacecraft and is bounded. For inertia matrix $\boldsymbol{J}$ is a positive matrix, i.e. $\boldsymbol{J} > 0$, we have $\Delta\boldsymbol{J} \neq -\boldsymbol{J}_0$. Furthermore

$$\boldsymbol{J}^{-1} = (\boldsymbol{J}_0 + \Delta\boldsymbol{J})^{-1} = \boldsymbol{J}_0^{-1} + \Delta\tilde{\boldsymbol{J}} \tag{18}$$

where $\Delta\tilde{\boldsymbol{J}} = -\boldsymbol{J}_0^{-1}\Delta\boldsymbol{J}(\boldsymbol{I}_3+\boldsymbol{J}_0^{-1}\Delta\boldsymbol{J})^{-1}\boldsymbol{J}_0^{-1}$. Taking (17) and (18) into the system (16), we can get

$$\begin{cases}\dot{\hat{\sigma}} = \boldsymbol{G}(\hat{\sigma})\hat{\boldsymbol{\omega}} + \boldsymbol{\delta}_1 \\ \dot{\hat{\boldsymbol{\omega}}} = -\boldsymbol{J}_0^{-1}\hat{\boldsymbol{\omega}}^{\times}(\boldsymbol{J}_0\hat{\boldsymbol{\omega}} + \boldsymbol{C}_0\boldsymbol{J}_w\boldsymbol{\Omega}) - \boldsymbol{J}_0^{-1}\boldsymbol{u} \\ +\boldsymbol{J}_0^{-1}\boldsymbol{u}_{g0} + \boldsymbol{\delta}_{21}\end{cases} \tag{19}$$

where

$$\begin{aligned}\boldsymbol{u}_{g0} &= 3\omega_0^2\boldsymbol{R}_3(\hat{\sigma}) \times \boldsymbol{J}_0\boldsymbol{R}_3(\hat{\sigma}) \\ \boldsymbol{\delta}_{21} &= -\Delta\tilde{\boldsymbol{J}}\hat{\boldsymbol{\omega}}^{\times}(\boldsymbol{J}_0\hat{\boldsymbol{\omega}} + \boldsymbol{C}_0\boldsymbol{J}_w\boldsymbol{\Omega}) - \boldsymbol{J}^{-1}\hat{\boldsymbol{\omega}}^{\times}\Delta\boldsymbol{J}\hat{\boldsymbol{\omega}} - \Delta\tilde{\boldsymbol{J}}\boldsymbol{u} \\ &\quad + \boldsymbol{\Delta}\tilde{\boldsymbol{J}}\boldsymbol{u}_g + 3\omega_0^2\boldsymbol{J}_0^{-1}\boldsymbol{R}_3(\sigma) \times \boldsymbol{\Delta}\boldsymbol{J}\boldsymbol{R}_3(\sigma) + \boldsymbol{J}^{-1}\boldsymbol{\delta}_{20}\end{aligned}$$

C. ACTUATOR FAULTS OR FAILURE

As shown in [23], the angular acceleration of reaction wheels $\dot{\boldsymbol{\Omega}}_w$ with actuator fault is established in the following uniform model

$$\dot{\boldsymbol{\Omega}}_w = \dot{\boldsymbol{\Omega}}_{wc} + \boldsymbol{B}(t, T_{fault})[(\boldsymbol{E}(t) - \boldsymbol{I}_4)\dot{\boldsymbol{\Omega}}_{wc} + \bar{\dot{\Omega}}_{wc}] \tag{20}$$

where $\dot{\boldsymbol{\Omega}}_{wc} = [\dot{\Omega}_{wc1}, \dot{\Omega}_{wc2}, \dot{\Omega}_{wc3}, \dot{\Omega}_{wc4}]$ represents the actuator command, $\bar{\dot{\Omega}}_{wc} = [\bar{\dot{\Omega}}_{wc1}, \bar{\dot{\Omega}}_{wc2}, \bar{\dot{\Omega}}_{wc3}, \bar{\dot{\Omega}}_{wc4}]^{\mathrm{T}}$ is the actuator bias; $\boldsymbol{E} = \mathrm{diag}\{e_1, e_2, e_3, e_4\}$ denotes the actuator effectiveness matrix. The matrix $\boldsymbol{B}(t, T_{fault}) \in \mathbb{R}^{4\times4}$ with $\boldsymbol{T}_{fault} = [t_1, t_2, t_3, t_4]^{\mathrm{T}}$ represents the time profiles of actuator faults, which is given by $\boldsymbol{B}(t, T_{fault}) = \mathrm{diag}\{b_1(t - t_1), b_2(t - t_2), b_3(t - t_3), b_4(t - t_4)\}$, where t_i is the fault occurrence time, and $b_i(t - t_i)$ denotes the time profile of a fault occurred on the i-th wheel, which is given by

$$b_i(t - t_i) = \begin{cases}0, & \text{if } t < t_i \\ 1 - e^{-a_i(t-t_i)}, & \text{if } t \geq t_i\end{cases} \tag{21}$$

where $a_i > 0$ represents the fault evolution rate. A small value of a_i indicates slowly occurrence faults, i.e. incipient faults. Otherwise, the time profile b_i denotes the abrupt faults.

Now define the control torque command $\boldsymbol{u}_c$ as

$$\boldsymbol{u}_c = \boldsymbol{C}\boldsymbol{J}_w\dot{\boldsymbol{\Omega}}_{wc}$$

and control torque bias $\bar{\boldsymbol{u}}_c$ as

$$\bar{\boldsymbol{u}}_c = \boldsymbol{C}\boldsymbol{J}_w\bar{\dot{\Omega}}_{wc}$$

Then the control torque $\boldsymbol{u}$ with actuator fault can be written as

$$\boldsymbol{u} = \boldsymbol{u}_c + \boldsymbol{C}\boldsymbol{J}_w\boldsymbol{B}(t, T_{fault})[(\boldsymbol{E}(t) - \boldsymbol{I}_4)\boldsymbol{D}\boldsymbol{u}_c + \boldsymbol{D}\bar{\boldsymbol{u}}_c] \tag{22}$$

where

$$\boldsymbol{D} = ((\boldsymbol{C}\boldsymbol{J}_w)^{\mathrm{T}}\boldsymbol{C}\boldsymbol{J}_w)^{-1}(\boldsymbol{C}\boldsymbol{J}_w)^{\mathrm{T}}$$

Hence, the attitude kinematics and dynamics with a general actuator fault model is given as follows

$$\begin{cases}\dot{\hat{\sigma}} = \boldsymbol{G}(\hat{\sigma})\hat{\boldsymbol{\omega}} + \boldsymbol{\delta}_1 \\ \dot{\hat{\boldsymbol{\omega}}} = -\boldsymbol{J}_0^{-1}\hat{\boldsymbol{\omega}}^{\times}(\boldsymbol{J}_0\hat{\boldsymbol{\omega}} + \boldsymbol{C}_0\boldsymbol{J}_w\boldsymbol{\Omega}_w) - \boldsymbol{J}_0^{-1}\boldsymbol{u}_c \\ -\boldsymbol{u}_\tau + \boldsymbol{J}_0^{-1}\boldsymbol{u}_{g0} + \boldsymbol{\delta}_{21}\end{cases} \tag{23}$$

where

$$\boldsymbol{u}_\tau = \boldsymbol{J}_0^{-1}\boldsymbol{C}\boldsymbol{J}_w\boldsymbol{B}(t, T_{fault})[(\boldsymbol{E}(t) - \boldsymbol{I}_4)\boldsymbol{D}\boldsymbol{u}_c + \boldsymbol{D}\bar{\boldsymbol{u}}_c]$$

D. ACTUATOR SATURATION

In practical applications, the control torque in the presence of saturation is a challenging problem. The signal $\boldsymbol{u}_c$ generated by the control torque cannot be implemented due to actuator saturation constraints. The control torque $\boldsymbol{u}_c$ with saturation constraint can be described as

$$u_{ci} = \begin{cases}u_{ci\max}, & \text{if } u_{0i} > u_{ci\max} \\ u_{0i}, & \text{if } u_{ci\min} \leq u_{0i} \leq u_{ci\max} \\ u_{ci\min}, & \text{if } u_{0i} < u_{ci\min},\end{cases} \quad i = 1, 2, 3$$

which can also be rewritten as

$$u_{ci} = u_{0i} + \Delta u_{ci}, \quad i = 1, 2, 3 \tag{24}$$

with

$$\Delta u_{ci} = \begin{cases}u_{ci\max} - u_{0i}, & \text{if } u_{0i} > u_{ci\max} \\ 0, & \text{if } u_{ci\min} \leq u_{0i} \leq u_{ci\max} \\ u_{ci\min} - u_0, & \text{if } u_{0i} < u_{ci\min}\end{cases}$$

with $i = 1, 2, 3$ and $\boldsymbol{u}_0 = [u_{01}, u_{02}, u_{03}]^{\mathrm{T}}$ is the control command to be designed in the presence of input saturation. Then the system (14) can be written as

$$\begin{cases}\dot{\hat{\sigma}} = \boldsymbol{G}(\hat{\sigma})\hat{\boldsymbol{\omega}} + \boldsymbol{\delta}_1, \\ \dot{\hat{\boldsymbol{\omega}}} = -\boldsymbol{J}_0^{-1}\hat{\boldsymbol{\omega}}^{\times}(\boldsymbol{J}_0\hat{\boldsymbol{\omega}} + \boldsymbol{C}_0\boldsymbol{J}_w\boldsymbol{\Omega}_w) \\ -\boldsymbol{J}_0^{-1}(\boldsymbol{u}_0 + \Delta\boldsymbol{u}_c) + \boldsymbol{J}_0^{-1}\boldsymbol{u}_{g0} + \boldsymbol{\delta}_2\end{cases} \tag{25}$$

where $\Delta\boldsymbol{u}_c = [\Delta u_{ci}, \Delta u_{c2}, \Delta u_3]^{\mathrm{T}}$ and $\boldsymbol{\delta}_2 = -\boldsymbol{u}_\tau + \delta_{21}$.

For system model (25), the following assumptions are employed in the subsequent development.

Assumption 4: The external disturbance $\boldsymbol{d}$ and its time derivative $\dot{\boldsymbol{d}}$ are bounded.

Assumption 5: The measurement uncertainties $\upsilon_i(t)$ and their time derivatives $\dot{\upsilon}_i(t)$ are also bounded such that $\|\upsilon_i(t)\| \leq l_{0i}$, $\|\dot{\upsilon}_i(t)\| \leq l_{1i}$ with unknown positive scalars l_{0i}, l_{1i} and $l_{2i}(i = 1, 2)$.

Assumption 6: Under the mild assumptions, $\|\Delta\boldsymbol{u}_c\|$ is always bounded by a scalar [31].

Remark 2: This assumption is reasonable according to the analysis in [31]. From the view of a practical control system, the difference $\Delta\boldsymbol{u}$ between the command control input $\boldsymbol{u}_0$ and the actual control input $\boldsymbol{u}_c$ cannot be large. The reason is that the system controllability should be satisfied when control input saturation occurs. And if the input difference $\Delta\boldsymbol{u}$ is too big, it means that the actuator cannot provide high enough control moment or control force to make the attitude control system stable in industry. From the controllability of a practical system, it is thus reasonable that $\Delta\boldsymbol{u}$ is always bounded by a constant. And the bound can be large to satisfy this assumption.

Assumption 7: For $\boldsymbol{\delta}_1$ and $\boldsymbol{\delta}_2$ are viewed as slowly varying signals with respect to the fast dynamics of disturbance observers under large observer gains, $\dot{\boldsymbol{\delta}}_1$ and $\dot{\boldsymbol{\delta}}_2$ are assumed as small bounded signals.

The attitude control problem of this study can be described by Fig. 3. Based on the model (25) and Assumption 1-7,

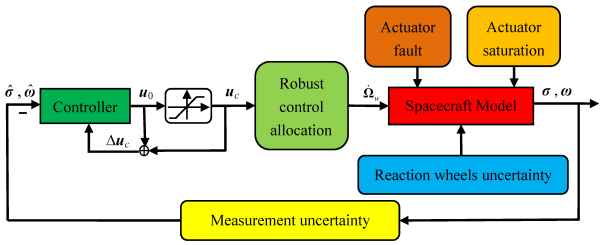

FIGURE 3. Flow chart of the developed control scheme for combined spacecraft.

the attitude stabilization control objective is stated formally as follows: for combined spacecraft attitude system with reaction wheels (25) in the presence of measurement uncertainties, inertia uncertainties, actuator fault and actuator saturation, to design a robust actuator such that the controlled spacecraft achieves that $\boldsymbol{\sigma}(t)$ and $\boldsymbol{\omega}(t)$ converge to a small neighborhood of zero as $t \to \infty$.

III. CONTROL LAW DESIGN

In this section, two steps are split for the controller design using the principle of robust control allocation: (1) A control law which produces the total control effort is designed, and (2) a robust control allocation method that maps the total control demand into individual reaction wheel torques is proposed.

A. DISTURBANCE-OBSERVER-BASED DYNAMIC SURFACE VIRTUAL CONTROL LAW

For the attitude control system of combined spacecraft with reaction wheels (25), a disturbance-observer-based dynamic surface control law is designed to achieve the control objectives.

Define the error surface as

$$\begin{cases} \boldsymbol{S}_1 = \hat{\boldsymbol{\sigma}} - \boldsymbol{x}_{1d} \\ \boldsymbol{S}_2 = \hat{\boldsymbol{\omega}} - \boldsymbol{x}_{2d} \end{cases} \tag{26}$$

where $\boldsymbol{x}_{1d} = 0$ and $\boldsymbol{x}_{2d}$ is the virtual control input. The design procedure is presented in two steps as follows.

Step 1: We start with the first equation in (25) by considering $\hat{\boldsymbol{\omega}}$ as a control input. The derivative of $\boldsymbol{S}_1$ is

$$\dot{\boldsymbol{S}}_1 = \boldsymbol{G}(\boldsymbol{S}_1)\hat{\boldsymbol{\omega}} + \boldsymbol{\delta}_1, \tag{27}$$

It is natural to determine the virtual control law $\bar{\boldsymbol{x}}_2$ into the following form

$$\bar{\boldsymbol{x}}_2 = -\boldsymbol{G}(\boldsymbol{S}_1)^{-1}(k_1\boldsymbol{S}_1 + \hat{\boldsymbol{\delta}}_1) \tag{28}$$

where k_1 is a positive constant, $\hat{\boldsymbol{\delta}}_1 = \boldsymbol{s} + \gamma\boldsymbol{S}_1$ with a positive constant γ and $\boldsymbol{s}$ is the output of the following nonlinear disturbance observer [32]

$$\dot{\boldsymbol{s}} = -\gamma\boldsymbol{s} - \gamma[\boldsymbol{G}(\boldsymbol{S}_1)\hat{\boldsymbol{\omega}} + \gamma\boldsymbol{S}_1] \tag{29}$$

Now using the idea of dynamic surface control, we pass $\bar{\boldsymbol{x}}_2$ through a first-order filter with time constant τ_2 to obtain a filtered virtual control $\boldsymbol{x}_{2d}$:

$$\tau_2\dot{\boldsymbol{x}}_{2d} + \boldsymbol{x}_{2d} = \bar{\boldsymbol{x}}_2, \quad \boldsymbol{x}_{2d}(0) = \bar{\boldsymbol{x}}_2(0) \tag{30}$$

and the boundary-layer error $\boldsymbol{y}_2$ and estimate error $\tilde{\boldsymbol{\delta}}_1$ are defined as

$$\boldsymbol{y}_2 = \boldsymbol{x}_{2d} - \bar{\boldsymbol{x}}_2 \tag{31}$$

$$\tilde{\boldsymbol{\delta}}_1 = \boldsymbol{\delta}_1 - \hat{\boldsymbol{\delta}}_1 \tag{32}$$

Considering the following augmented Lyapunov function candidate:

$$V_1 = \frac{1}{2}\boldsymbol{S}_1^{\mathrm{T}}\boldsymbol{S}_1 + \frac{1}{2}\tilde{\boldsymbol{\delta}}_1^{\mathrm{T}}\tilde{\boldsymbol{\delta}}_1 \tag{33}$$

the derivative of V_1 along the system trajectories is given by

$$\begin{aligned} \dot{V}_1 &= \boldsymbol{S}_1^{\mathrm{T}}\dot{\boldsymbol{S}}_1 + \tilde{\boldsymbol{\delta}}_1^{\mathrm{T}}\dot{\tilde{\boldsymbol{\delta}}}_1 \\ &= \boldsymbol{S}_1^{\mathrm{T}}(\boldsymbol{G}(\boldsymbol{S}_1)\hat{\boldsymbol{\omega}} + \boldsymbol{\delta}_1) + \tilde{\boldsymbol{\delta}}_1^{\mathrm{T}}(\dot{\boldsymbol{\delta}}_1 - \dot{\hat{\boldsymbol{\delta}}}_1) \\ &= \boldsymbol{S}_1^{\mathrm{T}}(\boldsymbol{G}(\boldsymbol{S}_1)\bar{\boldsymbol{x}}_2 + \boldsymbol{G}(\boldsymbol{S}_1)(\boldsymbol{S}_2 + \boldsymbol{y}_2) + \boldsymbol{\delta}_1) \\ &\quad + \tilde{\boldsymbol{\delta}}_1^{\mathrm{T}}(\dot{\boldsymbol{\delta}}_1 - \dot{\boldsymbol{s}} - \gamma\dot{\boldsymbol{S}}_1) \\ &= -\boldsymbol{S}_1^{\mathrm{T}}(k_1\boldsymbol{S}_1 + \hat{\boldsymbol{\delta}}_1) + \boldsymbol{S}_1^{\mathrm{T}}\boldsymbol{G}(\boldsymbol{S}_1)(\boldsymbol{S}_2 + \boldsymbol{y}_2) + \boldsymbol{S}_1^{\mathrm{T}}\boldsymbol{\delta}_1 \\ &\quad + \tilde{\boldsymbol{\delta}}_1^{\mathrm{T}}(\dot{\boldsymbol{\delta}}_1 + \gamma\boldsymbol{s} + \gamma(\boldsymbol{G}(\boldsymbol{S}_1)\hat{\boldsymbol{\omega}} + \gamma\boldsymbol{S}_1) - \gamma(\boldsymbol{G}(\boldsymbol{S}_1)\hat{\boldsymbol{\omega}} + \boldsymbol{\delta}_1)) \\ &= -k_1\boldsymbol{S}_1^{\mathrm{T}}\boldsymbol{S}_1 + \boldsymbol{S}_1^{\mathrm{T}}\tilde{\boldsymbol{\delta}}_1 + \boldsymbol{S}_1^{\mathrm{T}}(\boldsymbol{G}(\boldsymbol{S}_1)(\boldsymbol{S}_2 + \boldsymbol{y}_2)) \\ &\quad + \tilde{\boldsymbol{\delta}}_1^{\mathrm{T}}\dot{\boldsymbol{\delta}}_1 - \gamma\tilde{\boldsymbol{\delta}}_1^{\mathrm{T}}\tilde{\boldsymbol{\delta}}_1 \end{aligned} \tag{34}$$

Step 2: Proceeding to the second equation in (25), we design the control law $\boldsymbol{u}_0$ in this step. The derivative of $\boldsymbol{S}_2$ is

$$\begin{aligned} \dot{\boldsymbol{S}}_2 &= \dot{\hat{\boldsymbol{\omega}}} - \dot{\boldsymbol{x}}_{2d} \\ &= -\boldsymbol{J}_0^{-1}\hat{\boldsymbol{\omega}}^{\times}(\boldsymbol{J}_0\hat{\boldsymbol{\omega}} + \boldsymbol{C}_0\boldsymbol{J}_w\boldsymbol{\Omega}_w) - \boldsymbol{J}_0^{-1}\boldsymbol{u}_0 \\ &\quad - \boldsymbol{J}_0^{-1}\Delta\boldsymbol{u}_c + \boldsymbol{J}_0^{-1}\boldsymbol{u}_{g0} + \boldsymbol{\delta}_2 - \dot{\boldsymbol{x}}_{2d} \end{aligned} \tag{35}$$

Design the control input command for system model (25) as

$$\begin{aligned} \boldsymbol{u}_0 = \boldsymbol{J}_0[&\boldsymbol{G}^{\mathrm{T}}(\boldsymbol{S}_1)\boldsymbol{S}_1 - k_3\boldsymbol{J}_0^{-1}\boldsymbol{\zeta} \\ &- \boldsymbol{J}_0^{-1}\hat{\boldsymbol{\omega}}^{\times}(\boldsymbol{J}_0\hat{\boldsymbol{\omega}} + \boldsymbol{C}_0\boldsymbol{J}_w\boldsymbol{\Omega}_w) \\ &+ \boldsymbol{J}_0^{-1}\boldsymbol{u}_{g0} + k_2\boldsymbol{S}_2 + \hat{\boldsymbol{\delta}}_2 + \boldsymbol{y}_2/\tau_2] \end{aligned} \tag{36}$$

where $\boldsymbol{\zeta}$ is the output of the following antiwindup saturation compensator:

$$\dot{\boldsymbol{\zeta}} = -k_4\boldsymbol{\zeta} + \Delta\boldsymbol{u}_c \tag{37}$$

where k_4 is a positive constant, $\hat{\boldsymbol{\delta}}_2 = \boldsymbol{\eta} + \lambda\boldsymbol{S}_2$ with a positive constant and $\boldsymbol{\eta}$ is the output of the following nonlinear disturbance observer:

$$\begin{aligned} \dot{\boldsymbol{\eta}} = -\lambda\boldsymbol{\eta} - \lambda[&-\boldsymbol{J}_0^{-1}\hat{\boldsymbol{\omega}}^{\times}(\boldsymbol{J}_0\hat{\boldsymbol{\omega}} + \boldsymbol{C}_0\boldsymbol{J}_w\boldsymbol{\Omega}_w) \\ &- \boldsymbol{J}_0^{-1}\boldsymbol{u}_c + \boldsymbol{J}_0^{-1}\boldsymbol{u}_{g0} + \boldsymbol{y}_2/\tau_2 + \lambda\boldsymbol{S}_2] \end{aligned} \tag{38}$$

Let us define the estimate error $\tilde{\boldsymbol{\delta}}_2$ as

$$\tilde{\boldsymbol{\delta}}_2 = \boldsymbol{\delta}_2 - \hat{\boldsymbol{\delta}}_2 \tag{39}$$

and consider the following Lyapunov function candidate:

$$V_2 = \frac{1}{2}(\boldsymbol{S}_2^{\mathrm{T}}\boldsymbol{S}_2 + \boldsymbol{\zeta}^{\mathrm{T}}\boldsymbol{\zeta} + \tilde{\boldsymbol{\delta}}_2^{\mathrm{T}}\tilde{\boldsymbol{\delta}}_2) \tag{40}$$

then the derivative of V_2 along the system trajectories satisfies

$$\begin{aligned}\dot{V}_2 &= \boldsymbol{S}_2^{\mathrm{T}}\dot{\boldsymbol{S}}_2 + \boldsymbol{\zeta}^{\mathrm{T}}\dot{\boldsymbol{\zeta}} + \tilde{\boldsymbol{\delta}}_2^{\mathrm{T}}\dot{\tilde{\boldsymbol{\delta}}}_2 \\ &= \boldsymbol{S}_2^{\mathrm{T}}(-\boldsymbol{G}^{\mathrm{T}}(\boldsymbol{S}_1)\boldsymbol{S}_1 - k_2\boldsymbol{S}_2 + k_3\boldsymbol{J}_0^{-1}\boldsymbol{\zeta} - \boldsymbol{J}_0^{-1}\Delta\boldsymbol{u}_c + \tilde{\boldsymbol{\delta}}_2) \\ &\quad - k_4\boldsymbol{\zeta}^{\mathrm{T}}\boldsymbol{\zeta} + \boldsymbol{\zeta}^{\mathrm{T}}\Delta\boldsymbol{u}_c + \tilde{\boldsymbol{\delta}}_2^{\mathrm{T}}\dot{\tilde{\boldsymbol{\delta}}}_2 - \lambda\tilde{\boldsymbol{\delta}}_2^{\mathrm{T}}\tilde{\boldsymbol{\delta}}_2\end{aligned} \tag{41}$$

The closed-loop attitude dynamics control system of combined spacecraft with actuator saturation can be expressed as

$$\begin{cases}\dot{\boldsymbol{S}}_1 = \dot{\hat{\boldsymbol{\sigma}}} \\ \dot{\boldsymbol{S}}_2 = \dot{\hat{\boldsymbol{\omega}}} + \boldsymbol{y}_2/\tau_2 \\ \dot{\boldsymbol{y}}_2 = -\boldsymbol{y}_2/\tau_2 - \dot{\bar{\boldsymbol{x}}}_2 \\ \dot{\boldsymbol{\zeta}} = -k_4\boldsymbol{\zeta} + \Delta\boldsymbol{u}_c\end{cases} \tag{42}$$

with nonlinear disturbance observers (29) and (38). Then based on the dynamic surface control theory, the following theorem is proposed.

Theorem 1: Consider the combined spacecraft attitude model with reaction wheels (25) under Assumptions 1-7. If the parameters of controller (36) with nonlinear disturbance observer (29) and (38) satisfy $32k_1 \geq 9\tau_2, 2k_1\gamma \geq 3$, $\lambda k_2 \geq 2$ and $2k_2k_4 \geq 3k_3^2k_5^2$ where $k_5 = \left\|\boldsymbol{J}_0^{-1}\right\|$, and $k_i > 0 (i = 1, 2, 3, 4)$, then the attitude $\boldsymbol{\sigma}$ and the angular velocity $\boldsymbol{\omega}$ converge to a smaller neighborhood of zero by choosing suitable controller parameters.

Proof: It can be observed that there exits a continuous function μ such that

$$\left\|\dot{\bar{\boldsymbol{x}}}_2\right\| \leq \mu(\boldsymbol{S}_1, \boldsymbol{S}_2, \boldsymbol{y}_2, \tilde{\boldsymbol{\delta}}_2) \tag{43}$$

The Lyapunov function candidate of the whole attitude control system is taken as

$$V = V_1 + V_2 + V_3 \tag{44}$$

where $V_3 = \frac{1}{2}\boldsymbol{y}_2^{\mathrm{T}}\boldsymbol{y}_2$. The derivative of V along the system trajectories is given by

$$\begin{aligned}\dot{V} &= \dot{V}_1 + \dot{V}_2 + \dot{V}_3 \\ &\leq -k_1\boldsymbol{S}_1^{\mathrm{T}}\boldsymbol{S}_1 + \boldsymbol{S}_1^{\mathrm{T}}\tilde{\boldsymbol{\delta}}_1 + \boldsymbol{S}_1^{\mathrm{T}}\boldsymbol{G}(\boldsymbol{S}_1)\boldsymbol{S}_2 + \boldsymbol{S}_1^{\mathrm{T}}\boldsymbol{G}(\boldsymbol{S}_1)\boldsymbol{y}_2 \\ &\quad + \tilde{\boldsymbol{\delta}}_1^{\mathrm{T}}\dot{\tilde{\boldsymbol{\delta}}}_1 - \gamma\tilde{\boldsymbol{\delta}}_1^{\mathrm{T}}\tilde{\boldsymbol{\delta}}_1 - \boldsymbol{S}_2^{\mathrm{T}}\boldsymbol{G}^{\mathrm{T}}(\boldsymbol{S}_1)\boldsymbol{S}_1 - k_2\boldsymbol{S}_2^{\mathrm{T}}\boldsymbol{S}_2 \\ &\quad + k_3\boldsymbol{S}_2^{\mathrm{T}}\boldsymbol{J}_0^{-1}\boldsymbol{\zeta} - \boldsymbol{S}_2^{\mathrm{T}}\boldsymbol{J}_0^{-1}\Delta\boldsymbol{u}_c + \boldsymbol{S}_2^{\mathrm{T}}\tilde{\boldsymbol{\delta}}_2 \\ &\quad - k_4\boldsymbol{\zeta}^{\mathrm{T}}\boldsymbol{\zeta} + \boldsymbol{\zeta}^{\mathrm{T}}\Delta\boldsymbol{u}_c + \tilde{\boldsymbol{\delta}}_2^{\mathrm{T}}\dot{\tilde{\boldsymbol{\delta}}}_2 - \lambda\tilde{\boldsymbol{\delta}}_2^{\mathrm{T}}\tilde{\boldsymbol{\delta}}_2 + \boldsymbol{y}_2^{\mathrm{T}}(-\boldsymbol{y}_2/\tau_2 - \dot{\bar{\boldsymbol{x}}}_2) \\ &\leq -k_1\left\|\boldsymbol{S}_1\right\|^2 - k_2\left\|\boldsymbol{S}_2\right\|^2 - \gamma\left\|\tilde{\boldsymbol{\delta}}_1\right\|^2 - \lambda\left\|\tilde{\boldsymbol{\delta}}_2\right\|^2 \\ &\quad - k_4\left\|\boldsymbol{\zeta}\right\|^2 - \frac{1}{\tau_2}\left\|\boldsymbol{y}_2\right\|^2 + \left\|\boldsymbol{S}_1\right\|\left\|\tilde{\boldsymbol{\delta}}_1\right\| + \boldsymbol{S}_1^{\mathrm{T}}\boldsymbol{G}(\boldsymbol{S}_1)\boldsymbol{y}_2 \\ &\quad + \left\|\tilde{\boldsymbol{\delta}}_1\right\|\left\|\dot{\tilde{\boldsymbol{\delta}}}_1\right\| + k_3k_5\left\|\boldsymbol{S}_2\right\|\left\|\boldsymbol{\zeta}\right\| + k_5\left\|\boldsymbol{S}_2\right\|\left\|\Delta\boldsymbol{u}_c\right\| \\ &\quad + \left\|\boldsymbol{S}_2\right\|\left\|\tilde{\boldsymbol{\delta}}_2\right\| + \left\|\boldsymbol{\zeta}\right\|\left\|\Delta\boldsymbol{u}_c\right\| + \left\|\tilde{\boldsymbol{\delta}}_2\right\|\left\|\dot{\tilde{\boldsymbol{\delta}}}_2\right\| + \left\|\boldsymbol{y}_2\right\||\mu|\end{aligned}$$

because $1/4 \leq \|\boldsymbol{G}(\boldsymbol{S}_1)\| = \left\|(1 + \boldsymbol{\sigma}^{\mathrm{T}}\boldsymbol{\sigma})/4\right\| \leq 1/2$, then

$$\begin{aligned}\dot{V} &\leq -k_1\left\|\boldsymbol{S}_1\right\|^2 - k_2\left\|\boldsymbol{S}_2\right\|^2 - \gamma\left\|\tilde{\boldsymbol{\delta}}_1\right\|^2 - \lambda\left\|\tilde{\boldsymbol{\delta}}_2\right\|^2 - k_4\left\|\boldsymbol{\zeta}\right\|^2 \\ &\quad - \frac{1}{\tau_2}\left\|\boldsymbol{y}_2\right\|^2 + \left\|\boldsymbol{S}_1\right\|\left\|\tilde{\boldsymbol{\delta}}_1\right\| + (1/2)\left\|\boldsymbol{S}_1\right\|\left\|\boldsymbol{y}_2\right\| + \left\|\tilde{\boldsymbol{\delta}}_1\right\|\left\|\dot{\tilde{\boldsymbol{\delta}}}_1\right\| \\ &\quad + k_3k_5\left\|\boldsymbol{S}_2\right\|\left\|\boldsymbol{\zeta}\right\| + k_5\left\|\boldsymbol{S}_2\right\|\left\|\Delta\boldsymbol{u}_c\right\| + \left\|\boldsymbol{S}_2\right\|\left\|\tilde{\boldsymbol{\delta}}_2\right\| \\ &\quad + \left\|\boldsymbol{\zeta}\right\|\left\|\Delta\boldsymbol{u}_c\right\| + \left\|\tilde{\boldsymbol{\delta}}_2\right\|\left\|\dot{\tilde{\boldsymbol{\delta}}}_2\right\| + \left\|\boldsymbol{y}_2\right\||\mu| \\ &= \sum_{i=1}^{10}\Theta_i\end{aligned}$$

where

$$\begin{aligned}\Theta_1 &= -\frac{k_1}{3}\left\|\boldsymbol{S}_1\right\|^2 - \frac{k_2}{4}\left\|\boldsymbol{S}_2\right\|^2 - \frac{\gamma}{2}\left\|\tilde{\boldsymbol{\delta}}_1\right\|^2 \\ &\quad - \frac{\lambda}{2}\left\|\tilde{\boldsymbol{\delta}}_2\right\|^2 - \frac{2k_4}{3}\left\|\boldsymbol{\zeta}\right\|^2 - \frac{2}{3\tau_2}\left\|\boldsymbol{y}_2\right\|^2, \\ \Theta_2 &= -\frac{k_1}{3}(\left\|\boldsymbol{S}_1\right\| - \frac{3}{2k_1}\left\|\tilde{\boldsymbol{\delta}}_1\right\|)^2 + \frac{3}{4k_1}\left\|\tilde{\boldsymbol{\delta}}_1\right\|^2, \\ \Theta_3 &= -\frac{k_1}{3}(\left\|\boldsymbol{S}_1\right\| - \frac{3}{4k_1}\left\|\boldsymbol{y}_2\right\|)^2 + \frac{3}{16k_1}\left\|\boldsymbol{y}_2\right\|^2, \\ \Theta_4 &= -\frac{k_2}{4}(\left\|\boldsymbol{S}_2\right\| - \frac{2k_3k_5}{k_2}\left\|\boldsymbol{\zeta}\right\|)^2 + \frac{k_3^2k_5^2}{k_2}\left\|\boldsymbol{\zeta}\right\|^2, \\ \Theta_5 &= -\frac{k_2}{4}(\left\|\boldsymbol{S}_2\right\| - \frac{2k_5}{k_2}\left\|\Delta\boldsymbol{u}_c\right\|)^2 + \frac{k_5^2}{k_2}\left\|\Delta\boldsymbol{u}_c\right\|^2, \\ \Theta_6 &= -\frac{k_2}{4}(\left\|\boldsymbol{S}_2\right\| - \frac{2}{k_2}\left\|\tilde{\boldsymbol{\delta}}_2\right\|)^2 + \frac{1}{k_2}\left\|\tilde{\boldsymbol{\delta}}_2\right\|^2, \\ \Theta_7 &= -\frac{k_4}{3}(\left\|\boldsymbol{\zeta}\right\| - \frac{3}{2k_4}\left\|\Delta\boldsymbol{u}_c\right\|)^2 + \frac{3}{4k_4}\left\|\Delta\boldsymbol{u}_c\right\|^2, \\ \Theta_8 &= -\frac{1}{3\tau_2}(\left\|\boldsymbol{y}_2\right\| - \frac{3\tau_2}{2}|\mu|)^2 + \frac{3\tau_2}{4}|\mu|^2, \\ \Theta_9 &= -\frac{\gamma}{2}(\left\|\tilde{\boldsymbol{\delta}}_1\right\| - \frac{1}{\gamma}\left\|\dot{\tilde{\boldsymbol{\delta}}}_1\right\|)^2 + \frac{1}{2\gamma}\left\|\dot{\tilde{\boldsymbol{\delta}}}_1\right\|^2, \\ \Theta_{10} &= -\frac{\lambda}{2}(\left\|\tilde{\boldsymbol{\delta}}_2\right\| - \frac{1}{\lambda}\left\|\dot{\tilde{\boldsymbol{\delta}}}_2\right\|)^2 + \frac{1}{2\lambda}\left\|\dot{\tilde{\boldsymbol{\delta}}}_2\right\|^2\end{aligned}$$

then we can have

$$\begin{aligned}\dot{V} &\leq -\frac{k_1}{3}\left\|\boldsymbol{S}_1\right\|^2 - \frac{k_2}{4}\left\|\boldsymbol{S}_2\right\|^2 - (\frac{2k_4}{3} - \frac{k_3^2k_5^2}{k_2})\left\|\boldsymbol{\zeta}\right\|^2 \\ &\quad - (\frac{\gamma}{2} - \frac{3}{4k_1})\left\|\tilde{\boldsymbol{\delta}}_1\right\|^2 - (\frac{\lambda}{2} - \frac{1}{k_2})\left\|\tilde{\boldsymbol{\delta}}_2\right\|^2 \\ &\quad - (\frac{2}{3\tau_2} - \frac{3}{16k_1})\left\|\boldsymbol{y}_2\right\|^2 + (\frac{k_5^2}{k_2} + \frac{3}{4k_4})\left\|\Delta\boldsymbol{u}_c\right\|^2 \\ &\quad + \frac{3\tau_2}{4}|\mu|^2 + \frac{1}{2\gamma}\left\|\dot{\tilde{\boldsymbol{\delta}}}_1\right\|^2 + \frac{1}{2\lambda}\left\|\dot{\tilde{\boldsymbol{\delta}}}_2\right\|^2 \\ &\leq -\rho V + \epsilon\end{aligned} \tag{45}$$

where

$$\begin{aligned}\rho &= 2\min\{\frac{k_1}{3}, \frac{k_2}{4}, \frac{2k_4}{3} - \frac{k_3^2k_5^2}{k_2}, \frac{\gamma}{2} - \frac{3}{4k_1}, \frac{\lambda}{2} - \frac{1}{k_2}, \\ &\quad \frac{2}{3\tau_2} - \frac{3}{16k_1}\} > 0, \\ \epsilon &= (\frac{k_5^2}{k_2} + \frac{3}{4k_4})\left\|\Delta\boldsymbol{u}_c\right\|^2 + \frac{3\tau_2}{4}|\mu|^2 + \frac{1}{2\gamma}\left\|\dot{\tilde{\boldsymbol{\delta}}}_1\right\|^2 + \frac{1}{2\lambda}\left\|\dot{\tilde{\boldsymbol{\delta}}}_2\right\|^2\end{aligned}$$

Then according to the comparison principle, we have $V(t) \leq V(t_0)e^{-\rho t} + \frac{1}{\rho}\|\epsilon\|$. Now consider the set $A = \{\boldsymbol{S}_1, \boldsymbol{S}_2, \tilde{\boldsymbol{\delta}}_1, \tilde{\boldsymbol{\delta}}_2, \boldsymbol{y}_2 : V \leq p\}$. Because A is a compact set, there exist maximum value of $\mu(\boldsymbol{S}_1, \boldsymbol{S}_2, \boldsymbol{y}_2, \tilde{\boldsymbol{\delta}}_2)$ on A. Also,

according to Assumptions 6-7, we have $\|\Delta \boldsymbol{u}_c\|$, $\dot{\boldsymbol{\delta}}_1$ and $\dot{\tilde{\boldsymbol{\delta}}}_1$ are bounded by scalars. Thus, $\|\epsilon\| \leq \xi$ can be derived with an unknown scalar ξ. Then we can obtain that $\dot{V} \leq -\rho V + \xi$ which lead to $\lim_{t\to\infty} V(t) \leq \frac{\xi}{\rho}$. According to the definition of $V(t)$, the error surface $\|\boldsymbol{S}_1\|$ and $\|\boldsymbol{S}_2\|$, saturation compensator $\|\boldsymbol{\zeta}\|$, the boundary-layer error $\|\boldsymbol{y}_2\|$ and the disturbance estimate error $\left\|\tilde{\boldsymbol{\delta}}_1\right\|$ and $\left\|\tilde{\boldsymbol{\delta}}_2\right\|$ converge to a small neighborhood of zero when $t \to \infty$. Furthermore, since $\boldsymbol{S}_1 = \hat{\boldsymbol{\sigma}}$, $\boldsymbol{S}_2 = \hat{\boldsymbol{\omega}} - \boldsymbol{x}_{2d} = \hat{\boldsymbol{\omega}} - \bar{\boldsymbol{x}}_2 - \boldsymbol{y}_2$, $\bar{\boldsymbol{x}}_2 = -\boldsymbol{G}(\boldsymbol{S}_1)^{-1}(k_1\boldsymbol{S}_1 + \hat{\boldsymbol{\delta}}_1)$, $2 \leq \left\|\boldsymbol{G}(\boldsymbol{S}_1)^{-1}\right\| \leq 4$ and $\left\|\hat{\boldsymbol{\delta}}_1\right\| \leq \|\boldsymbol{\delta}_1\| + \left\|\tilde{\boldsymbol{\delta}}_1\right\|$, then we have

$$\begin{aligned}
\left\|\hat{\boldsymbol{\sigma}}\right\| &= \|\boldsymbol{S}_1\| \leq \sqrt{2p^*} \\
\left\|\hat{\boldsymbol{\omega}}\right\| &\leq \|\boldsymbol{S}_2\| + \left\|\boldsymbol{y}_2\right\| + \|\bar{\boldsymbol{x}}_2\| \\
&\leq \|\boldsymbol{S}_2\| + \left\|\boldsymbol{y}_2\right\| + 4(k_1\|\boldsymbol{S}_1\| + \|\boldsymbol{\delta}_1\| + \left\|\tilde{\boldsymbol{\delta}}_1\right\|) \\
&\leq (4k_1 + 6)\sqrt{2p^*} + \|\boldsymbol{\delta}_1\|
\end{aligned}$$

Because of

$$\|\boldsymbol{\delta}_1\| \leq c_1\left\|\hat{\boldsymbol{\omega}}\right\| + c_2$$

with $c_1 = (\sqrt{2p^*} + \frac{1}{2})l_{01} + \frac{1}{2}l_{01}^2$ and $c_2 = \frac{1}{2}l_{02} + l_{11}$, then

$$\left\|\hat{\boldsymbol{\omega}}\right\| \leq \frac{1}{1-c_1}[(4k_1 + 6)\sqrt{2p^*} + c_2]$$

Furthermore, from (15) and Assumption 5, we have

$$\begin{aligned}
\|\boldsymbol{\sigma}\| &\leq \left\|\hat{\boldsymbol{\sigma}}\right\| + \|\boldsymbol{v}_1\| \leq \sqrt{2p^*} + l_{01} \\
\|\boldsymbol{\omega}\| &\leq \left\|\hat{\boldsymbol{\omega}}\right\| + \|\boldsymbol{v}_2\| \leq \frac{1}{1-c_1}[(4k_1 + 6)\sqrt{2p^*} + c_2] + l_{02}
\end{aligned}$$

then because p^* can be made small enough, the bounds of $\sigma(t)$ and $\omega(t)$ can also be small. ■

Remark 3: Since the convergence rate of the system states is mainly determined by ρ, larger ρ results in faster convergence rate. And ρ is related to controller, saturation compensator, observer and filter parameters $k_1, k_2, k_3, k_4, \gamma, \lambda$ and τ, larger $k_1, k_2, k_4, \gamma, \lambda$ and smaller k_3,τ lead to larger ρ and faster convergence rate of attitude. Also, the ultimate bounds of attitude and angular velocity are related to the bounds of measurement uncertainties, which means that the attitude control performance is mainly determined by both control strategy and measurement precision.

Remark 4: Comparing with the backstepping method in [6], dynamic surface method is proposed in this paper. We note that the proposed control law does not involve the differentiation of $\boldsymbol{G}(\boldsymbol{S}_1)^{-1}$ and thus has prevented the explosion of terms. Also, the term $\boldsymbol{J}_0^{-1}\Delta\boldsymbol{u}_c$ is not contained in the new disturbance $\boldsymbol{\delta}_2$, which means that the burden of observer can be alleviated dramatically, the precision and accuracy of the controller can be improved ulteriorly.

B. ROBUST CONTROL ALLOCATION

In this section, an approach to map the virtual control to each reaction wheel is presented. The robust control allocation problem including saturation constraints is given. Due to physical limitations on reaction wheels, it is crucial to redistribute the control efforts among each reaction wheel in the frame $\mathcal{F}_c(O_c x_c y_c z_c)$. In reality, the limitations on the command angular acceleration of reaction wheels $\dot{\boldsymbol{\Omega}}_{wc}$ is assumed as

$$\dot{\boldsymbol{\Omega}}_{wc} \in \mathcal{U} = \{\dot{\boldsymbol{\Omega}}_{wc} | \dot{\boldsymbol{\Omega}}_{wc\,\min} \leq \dot{\boldsymbol{\Omega}}_{wc} \leq \dot{\boldsymbol{\Omega}}_{wc\,\max}\} \tag{46}$$

where $\dot{\boldsymbol{\Omega}}_{wc\,\min} = \left[\dot{\Omega}_{wc1\,\min}, \dot{\Omega}_{wc2\,\min}, \dot{\Omega}_{wc3\,\min}, \dot{\Omega}_{wc4\,\min}\right]^{\mathrm{T}}$ and $\dot{\boldsymbol{\Omega}}_{wc\,\max} = \left[\dot{\Omega}_{wc1\,\max}, \dot{\Omega}_{wc2\,\max}, \dot{\Omega}_{wc3\,\max}, \dot{\Omega}_{wc4\,\max}\right]^{\mathrm{T}}$.

In this paper, the virtual control torque $\boldsymbol{u}_c \in \mathbb{R}^3$ is designed to specify total attitude control torque. Now look at equation (8), assume that

$$\boldsymbol{R}_{sc} = \begin{bmatrix} r_{11} & r_{12} & r_{13} \\ r_{21} & r_{22} & r_{23} \\ r_{31} & r_{32} & r_{33} \end{bmatrix}, \quad \Delta\boldsymbol{r}_c = \begin{bmatrix} \Delta r_{c1} \\ \Delta r_{c2} \\ \Delta r_{c3} \end{bmatrix}$$

then $\Delta\boldsymbol{C}$ can be written as

$$\Delta\boldsymbol{C} = \Delta r_{c1}\boldsymbol{C}_1 + \Delta r_{c2}\boldsymbol{C}_2 + \Delta r_{c3}\boldsymbol{C}_3 \tag{47}$$

with

$$\boldsymbol{C}_1 = \begin{bmatrix} r_{11} & r_{11} & r_{11} & r_{11} \\ r_{21} & r_{21} & r_{21} & r_{21} \\ r_{31} & r_{31} & r_{31} & r_{31} \end{bmatrix}$$

$$\boldsymbol{C}_2 = \begin{bmatrix} r_{12} & r_{12} & r_{12} & r_{12} \\ r_{22} & r_{22} & r_{22} & r_{22} \\ r_{32} & r_{32} & r_{32} & r_{32} \end{bmatrix}$$

$$\boldsymbol{C}_3 = \begin{bmatrix} r_{12} & r_{12} & r_{12} & r_{12} \\ r_{22} & r_{22} & r_{22} & r_{22} \\ r_{32} & r_{32} & r_{32} & r_{32} \end{bmatrix}$$

It can be assumed that $\Delta\boldsymbol{r}_c$ satisfies $\Delta_i^- \leq \Delta r_{ci} \leq \Delta_i^+$. Define

$$\Delta_I = \left\{\Delta r_c | \Delta r_{ci} \in \left[\Delta_i^-, \Delta_i^+\right], i = 1, 2, 3\right\} \tag{48}$$

then the robust control allocation (RobCA) problem is defined as:

$$\dot{\boldsymbol{\Omega}}_{wc} = \arg\min_{\dot{\boldsymbol{\Omega}}_{wc}\in\Theta} \left\|\dot{\boldsymbol{\Omega}}_{wc}\right\|_{\boldsymbol{M}_1}^2 \tag{49}$$

with

$$\Theta = \arg\min_{\dot{\boldsymbol{\Omega}}_{wc}\in\mathcal{U}} \max_{\Delta r_c\in\Delta_I} \left\|\boldsymbol{u}_c - (\boldsymbol{C}_0 + \Delta\boldsymbol{C}(\Delta r_c))\boldsymbol{J}_w\dot{\boldsymbol{\Omega}}_{wc}\right\|^2 \tag{50}$$

where $\left\|\dot{\boldsymbol{\Omega}}_{wc}\right\|_{\boldsymbol{M}_1}^2$ stands for $\dot{\boldsymbol{\Omega}}_{wc}^{\mathrm{T}}\boldsymbol{M}_1\dot{\boldsymbol{\Omega}}_{wc}$ and the weighting matrix $\boldsymbol{M}_1 = \mathrm{diag}\{m_{11}, m_{12}, m_{13}, m_{14}\}$. Furthermore, RobCA can be rewritten as

$$\begin{aligned}
\dot{\boldsymbol{\Omega}}_{wc} = \arg\min_{\dot{\boldsymbol{\Omega}}_{wc}\in\mathcal{U}} \max_{\Delta r_c\in\Delta_I} \{&\left\|\dot{\boldsymbol{\Omega}}_{wc}\right\|_{\boldsymbol{M}_1}^2 \\
&+ h\left\|\boldsymbol{u}_c - (\boldsymbol{C}_0 + \Delta\boldsymbol{C}(\Delta r_c))\boldsymbol{J}_w\dot{\boldsymbol{\Omega}}_{wc}\right\|^2\}
\end{aligned} \tag{51}$$

where h is a given positive scalar. The following result can be obtained.

Theorem 2: If $\Delta\boldsymbol{r}_c \in \Delta_I$, the RobCA problem has an optimal solution if the following is solved for any $\Delta\boldsymbol{r}_c \in \Delta_E$

$$\begin{aligned}
&\min_{\dot{\boldsymbol{\Omega}}_{wc}} \Upsilon \\
&\text{s.t. } \Upsilon_1 + \Upsilon_2 - \Upsilon < 0
\end{aligned} \tag{52}$$

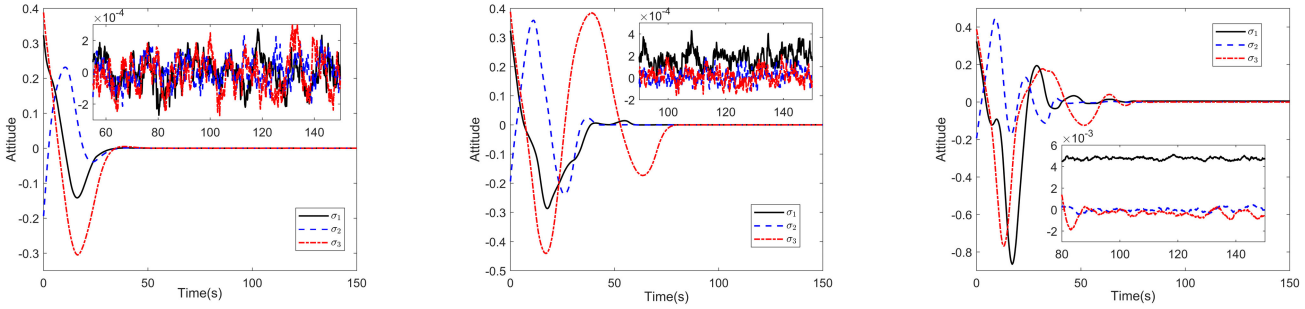

(a) Proposed controller (b) RFTFT controller (c) PD controller

FIGURE 4. Time history of attitude.

$$\begin{bmatrix} -\boldsymbol{I} & \boldsymbol{M}_1^{1/2}\dot{\boldsymbol{\Omega}}_{wc} \\ (\boldsymbol{M}_1^{1/2}\dot{\boldsymbol{\Omega}}_{wc})^{\mathrm{T}} & -\Upsilon_1\boldsymbol{I} \end{bmatrix} < 0 \tag{53}$$

$$\begin{bmatrix} -\boldsymbol{I} & \boldsymbol{\Psi}_{12} \\ \boldsymbol{\Psi}_{12}^{\mathrm{T}} & -\Upsilon_2\boldsymbol{I} \end{bmatrix} < 0 \tag{54}$$

$$\begin{bmatrix} \boldsymbol{b}_1^{\mathrm{T}}\boldsymbol{\Psi}_2 & 0 & 0 & 0 \\ 0 & \boldsymbol{b}_2^{\mathrm{T}}\boldsymbol{\Psi}_2 & 0 & 0 \\ 0 & 0 & \boldsymbol{b}_3^{\mathrm{T}}\boldsymbol{\Psi}_2 & 0 \\ 0 & 0 & 0 & \boldsymbol{b}_4^{\mathrm{T}}\boldsymbol{\Psi}_2 \end{bmatrix} < 0 \tag{55}$$

$$\begin{bmatrix} \boldsymbol{b}_1^{\mathrm{T}}\boldsymbol{\Psi}_3 & 0 & 0 & 0 \\ 0 & \boldsymbol{b}_2^{\mathrm{T}}\boldsymbol{\Psi}_3 & 0 & 0 \\ 0 & 0 & \boldsymbol{b}_3^{\mathrm{T}}\boldsymbol{\Psi}_3 & 0 \\ 0 & 0 & 0 & \boldsymbol{b}_4^{\mathrm{T}}\boldsymbol{\Psi}_3 \end{bmatrix} < 0 \tag{56}$$

where

$$\begin{aligned} \boldsymbol{\Psi}_{12} &= \sqrt{h}(\boldsymbol{u}_c - (\boldsymbol{C}_0 + \Delta\boldsymbol{C}(\Delta r_c))\boldsymbol{J}_w\dot{\boldsymbol{\Omega}}_{wc}), \\ \boldsymbol{\Psi}_2 &= \dot{\boldsymbol{\Omega}}_{wc\,\min} - \dot{\boldsymbol{\Omega}}_{wc}, \\ \boldsymbol{\Psi}_3 &= \dot{\boldsymbol{\Omega}}_{wc} - \dot{\boldsymbol{\Omega}}_{wc\,\max} \end{aligned}$$

and $\Upsilon > 0$, $\Upsilon_1 > 0$, $\Upsilon_2 > 0$, $\boldsymbol{b}_i (i = 1, 2, 3, 4)$ are unit column vectors and satisfy $[\boldsymbol{b}_1, \boldsymbol{b}_2, \boldsymbol{b}_3, \boldsymbol{b}_4] = \boldsymbol{I}_4$, and $\Delta_E = \{\Delta\boldsymbol{r}_c | \Delta r_{ci} = \Delta_i^- \text{ or } \Delta_i^+, i = 1, 2, 3\}$.

Proof: Denote

$$\begin{aligned} \Upsilon_1 &= \left\|\dot{\boldsymbol{\Omega}}_{wc}\right\|_{\boldsymbol{M}_1}^2, \\ \Upsilon_2 &= h\left\|\boldsymbol{u}_c - (\boldsymbol{C}_0 + \Delta\boldsymbol{C}(\Delta r_c))\boldsymbol{J}_w\dot{\boldsymbol{\Omega}}_{wc}\right\|^2 \end{aligned}$$

To ensure

$$\max_{\Delta r_c \in \Delta_I} \{\left\|\dot{\boldsymbol{\Omega}}_{wc}\right\|_{\boldsymbol{M}_1}^2 + h\left\|\boldsymbol{u}_c - (\boldsymbol{C}_0 + \Delta\boldsymbol{C}(\Delta r_c))\boldsymbol{J}_w\dot{\boldsymbol{\Omega}}_{wc}\right\|^2\} < \Upsilon$$

it holds if

$$\Upsilon_1 + \Upsilon_2 < \Upsilon$$

and

$$\dot{\boldsymbol{\Omega}}_{wc}^{\mathrm{T}}\boldsymbol{M}_1\dot{\boldsymbol{\Omega}}_{wc} < \Upsilon_1, \tag{57}$$

$$\boldsymbol{\Psi}_{12}^{\mathrm{T}}\boldsymbol{\Psi}_{12} < \Upsilon_2 \tag{58}$$

Using the Schur complement Lemma, (57) and (58) are equal to

$$\begin{bmatrix} -\boldsymbol{I} & \boldsymbol{M}_1^{1/2}\dot{\boldsymbol{\Omega}}_{wc} \\ (\boldsymbol{M}_1^{1/2}\dot{\boldsymbol{\Omega}}_{wc})^{\mathrm{T}} & -\Upsilon_1\boldsymbol{I} \end{bmatrix} < 0$$

$$\begin{bmatrix} -\boldsymbol{I} & \boldsymbol{\Psi}_{12} \\ \boldsymbol{\Psi}_{12}^{\mathrm{T}} & -\Upsilon_2\boldsymbol{I} \end{bmatrix} < 0$$

for $\Delta r_c \in \Delta_I$, then according to Corollary 4.3.1 in [33], (54) is obtained. To add the constraint to $\dot{\boldsymbol{\Omega}}_{wc}$, we have

$$\begin{aligned} &\dot{\boldsymbol{\Omega}}_{wc\,\min} < \dot{\boldsymbol{\Omega}}_{wc} < \dot{\boldsymbol{\Omega}}_{wc\,\max} \\ &\Longleftrightarrow \begin{bmatrix} \dot{\Omega}_{wc1\,\min} \\ \dot{\Omega}_{wc2\,\min} \\ \dot{\Omega}_{wc3\,\min} \\ \dot{\Omega}_{wc4\,\min} \end{bmatrix} < \begin{bmatrix} \dot{\Omega}_{wc1} \\ \dot{\Omega}_{wc2} \\ \dot{\Omega}_{wc3} \\ \dot{\Omega}_{wc4} \end{bmatrix} < \begin{bmatrix} \dot{\Omega}_{wc1\,\max} \\ \dot{\Omega}_{wc2\,\max} \\ \dot{\Omega}_{wc3\,\max} \\ \dot{\Omega}_{wc4\,\max} \end{bmatrix} \end{aligned} \tag{59}$$

then rewrite left side of (59) as:

$$\begin{bmatrix} \dot{\Omega}_{wc1\,\min} \\ \dot{\Omega}_{wc2\,\min} \\ \dot{\Omega}_{wc3\,\min} \\ \dot{\Omega}_{wc4\,\min} \end{bmatrix} < \begin{bmatrix} \dot{\Omega}_{wc1} \\ \dot{\Omega}_{wc2} \\ \dot{\Omega}_{wc3} \\ \dot{\Omega}_{wc4} \end{bmatrix}$$

$$\Longleftrightarrow \begin{bmatrix} \Psi_{21} & 0 & 0 & 0 \\ 0 & \Psi_{22} & 0 & 0 \\ 0 & 0 & \Psi_{23} & 0 \\ 0 & 0 & 0 & \Psi_{24} \end{bmatrix} < 0$$

$$\Longleftrightarrow \begin{bmatrix} \boldsymbol{b}_1^{\mathrm{T}}\boldsymbol{\Psi}_2 & 0 & 0 & 0 \\ 0 & \boldsymbol{b}_2^{\mathrm{T}}\boldsymbol{\Psi}_2 & 0 & 0 \\ 0 & 0 & \boldsymbol{b}_3^{\mathrm{T}}\boldsymbol{\Psi}_2 & 0 \\ 0 & 0 & 0 & \boldsymbol{b}_4^{\mathrm{T}}\boldsymbol{\Psi}_2 \end{bmatrix} < 0$$

with $\Psi_{2i} = \dot{\Omega}_{wci\,\min} - \dot{\Omega}_{wci}$, $i = 1, 2, 3, 4$. Thus (55) can be obtained, by the same way, we can also get (56). ■

IV. SIMULATION

In this experiment, the dynamic model of combined spacecraft system consists of a service spacecraft, a target spacecraft and one 3-DOF space manipulator. The involved differential equations in preceding sections were integrated using a fixed-step Runge–Kutta solver (0.1 s).

The inertia matrix of the combined spacecraft is set as $\boldsymbol{J} = \mathrm{diag}\{12, 14, 22\}\mathrm{kg}\cdot\mathrm{m}^2$, the nominal inertia matrix is $\boldsymbol{J}_0 = \mathrm{diag}\{10, 15, 20\}\mathrm{kg}\cdot\mathrm{m}^2$ [6]. For each reaction wheel, the inertia is 0.338 $\mathrm{kg}\cdot\mathrm{m}^2$, the maximum and minimum value on the angular acceleration vector of reaction wheels are $\dot{\Omega}_{wci\,\max} = 7$ and $\dot{\Omega}_{wci\,\min} = -7\ \mathrm{rad/s}^2$, $i = 1, 2, 3, 4$. According to the control mapping relationship between angular acceleration $\dot{\boldsymbol{\Omega}}_{wc}$ and virtual control torque $\boldsymbol{u}_c$, the limitations on the control input torque are set as $u_{ci\,\max} = 1$ and $u_{ci\,\min} = -1\,\mathrm{Nm}$ $(i = 1, 2, 3)$ (Note that $u_{ci\,\max}$ and $u_{ci\,\max}$ are selected such that the angular acceleration of reaction wheels

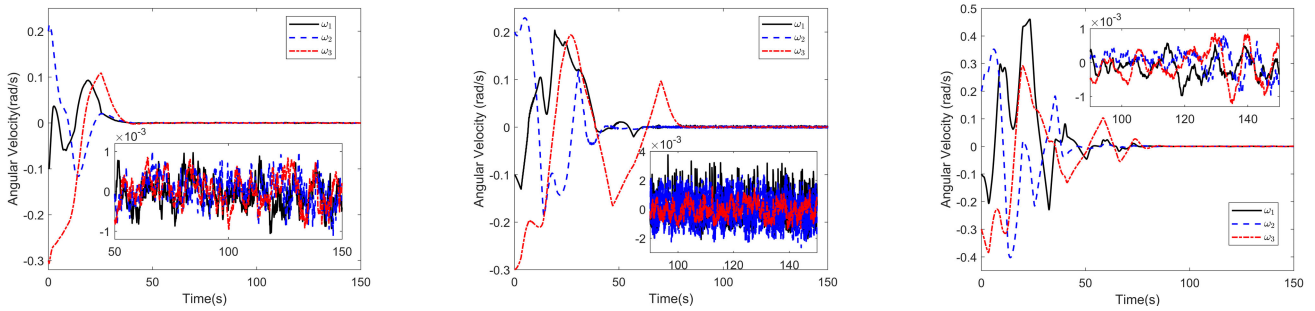

(a) Proposed controller (b) RFTFT controller (c) PD controller

FIGURE 5. Time history of angular velocity.

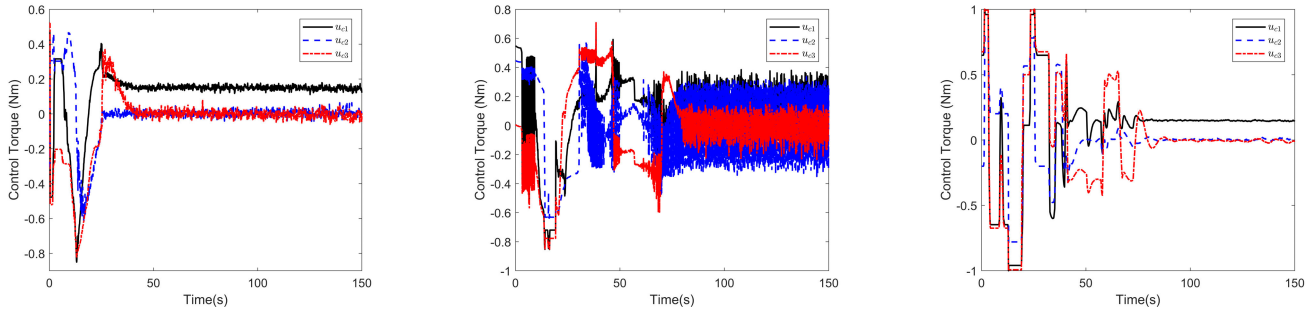

(a) Proposed controller (b) RFTFT controller (c) PD controller

FIGURE 6. Time history of control torque.

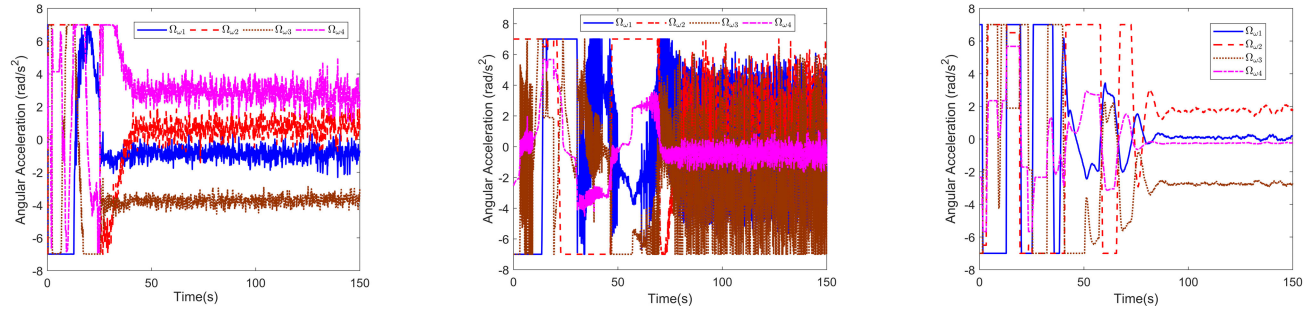

(a) Proposed controller (b) RFTFT controller (c) PD controller

FIGURE 7. Time history of angular acceleration of reaction wheels.

$\dot{\boldsymbol{\Omega}}_{wc}$ is obtained satisfying $\boldsymbol{u}_c = \boldsymbol{C}\boldsymbol{J}_w\dot{\boldsymbol{\Omega}}_{wc}$ and $\dot{\Omega}_{wci\min} \le \dot{\Omega}_{wci} \le \dot{\Omega}_{wci\max}$, $i = 1, 2, 3, 4$). The reaction wheels' configuration matrix of the service spacecraft expressed in the frame $\mathcal{F}_s(O_s x_s y_s z_s)$ is set as

$$\bar{\boldsymbol{C}} = \begin{bmatrix} 1 & 0 & 0 & 1/\sqrt{3} \\ 0 & 1 & 0 & 1/\sqrt{3} \\ 0 & 0 & 1 & 1/\sqrt{3} \end{bmatrix}$$

The rotation matrix $\boldsymbol{R}_{sc}$ is set as

$$\boldsymbol{R}_{sc} = \begin{bmatrix} 0.63708 & 0.63708 & -0.43388 \\ -0.87855 & 0.61925 & 0.78026 \\ 0.76577 & -0.45897 & 0.45048 \end{bmatrix}$$

and the nominal vector $\boldsymbol{r}_{c0}$ is defined as $\boldsymbol{r}_c = [2, 2, 2]^T$ m. We assume that the measurement error $\Delta\boldsymbol{r}_c$ satisfying $|\ \Delta r_{ci}\ | \le 0.3$ ($i = 1, 2, 3$), then according to equation (7) and (8), the nominal configuration matrix $\boldsymbol{C}_0$ and uncertain one $\Delta\boldsymbol{C}$ expressed in the body frame of combined spacecraft are

$$\boldsymbol{C}_0 = \begin{bmatrix} -1.04348 & -1.04348 & -2.11444 & -1.19542 \\ -1.92047 & -4.22670 & -2.61660 & -7.41144 \\ -7.4879 & -1.97353 & -1.06408 & -1.07734 \end{bmatrix}$$

$$\Delta\boldsymbol{C} = \begin{bmatrix} 0.16801 & 0.16801 & 0.16801 & 0.16801 \\ 0.10419 & 0.10419 & 0.10419 & 0.10419 \\ 0.15146 & 0.15146 & 0.15146 & 0.15146 \end{bmatrix}$$

Also, the actuator fault is considered as follows: the first control torque undergoes $e_1 = 0.5$ and $\bar{u}_2 = 0.2$ Nm after 5 s; the second control torque undergoes $e_2 = 0.5$ after 10 s; the

TABLE 1. Main control gains for simulations.

Controllers	Controller gains
Proposed controller	$k_1 = 0.5$, $k_2 = 0.4$, $k_3 = 0.05$, $k_4 = 20$, $\gamma = 10$, $\lambda = 4$, $\tau = 1$
PD controller	$\beta_1 = 14$, $\beta_2 = 15$
RFTFT controller	$\gamma = 0.7$, $\Gamma = \text{diag}([0.5; 0.5; 0.5])$, $\rho = 0.4$, $k_1 = \text{diag}([1; 1; 1])$, $k_2 = \text{diag}([4; 4; 4])$

third control torque experiences $e_3 = 0$ and $\bar{u}_3 = -0.2$ Nm from 5 s to 15 s. The fault evolution rate $a_i = 1$, $i = 1, 2, 3, 4$.

The combined spacecraft is assumed to be tumbling, the initial attitude MPR of combined spacecraft is set as $\boldsymbol{\sigma}(0) = [0.323, -0.194, 0.388]^{\mathrm{T}}$, the initial angular velocity $\boldsymbol{\omega}(0) = [-0.01, 0.02, -0.03]^{\mathrm{T}}$, and the measurement errors are also defined as [6]

$$\begin{cases} \boldsymbol{\upsilon}_1 = \delta_{s1}\boldsymbol{\sigma} + \boldsymbol{\delta}_{n1} \\ \boldsymbol{\upsilon}_2 = \delta_{s2}\boldsymbol{\omega} + \boldsymbol{\delta}_{n2} \end{cases} \tag{60}$$

where $\boldsymbol{\delta}_{n1} = [\delta_{n11}, \delta_{n12}, \delta_{n13}]^T$ and $\boldsymbol{\delta}_{n2} = [\delta_{n21}, \delta_{n22}, \delta_{n23}]^T$, and δ_{si}, δ_{nij} ($i = 1, 2$, $j = 1, 2, 3$) are both Gaussian white noise. Here, we set mean value and standard deviation of δ_{s_i} ($i = 1, 2$) as zeros and 0.005 respectively, mean value and standard deviation of δ_{nij} ($i = 1, 2$, $j = 1, 2, 3$) as zeros and 0.002 respectively. The external disturbance model is in the form of [34]

$$\boldsymbol{d} = \begin{bmatrix} 0.005\cos(0.02t) \\ -0.005\cos(0.025t) \\ 0.006\sin(0.04t) \end{bmatrix} \text{Nm}$$

In the following subsections, in order to show the superiority of the proposed control scheme, traditional PD controller $u_c = -\beta_1\boldsymbol{\sigma} - \beta_2\boldsymbol{\omega}$ [35] and the robust finite-time fault-tolerant controller (RFTFT) in [36] are conducted. The gains of those control algorithms were selected as shown in Table 1. Note that the control gains selected in this paper were chosen using trial and error until a satisfactory simulation result is obtained.

A. EFFECTIVENESS AND SUPERIORITY OF THE WHOLE CONTROL SCHEME

In this subsection, in order to show the effectiveness and superiority of the proposed nonlinear disturbance-observer-based dynamic surface controller with robust LMI-based control allocation method, the PD controller and RFTFT controller with psuedo-inverse control allocation method are implemented for the purpose of comparison. The simulation results are shown in Fig. 4-9. Fig. 4 presents the time history of the attitude trajectories. Fig. 5 presents the time history of the angular velocity trajectories. Fig. 6 presents the time history of control torque. Fig. 7 presents the time history of angular acceleration of reaction wheels. Fig. 8 presents the time history of states of two disturbance observers in proposed controller. Fig. 9 presents the time history of two estimation errors in proposed controller.

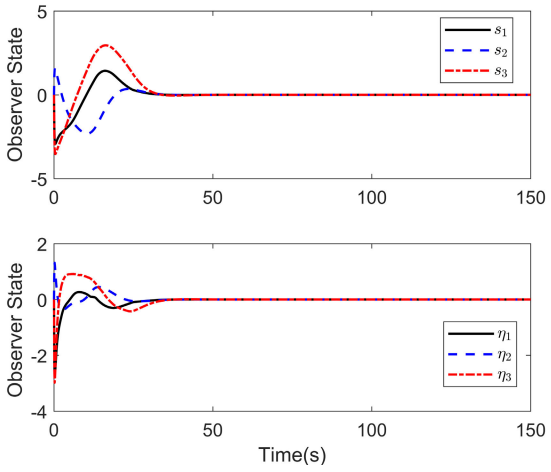

FIGURE 8. Time response of states of two disturbance observers.

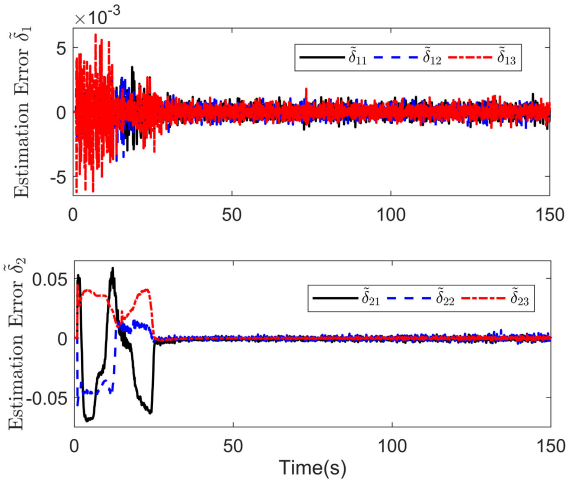

FIGURE 9. Time response of two estimation errors.

In Fig. 4, the magnitude of attitude with the proposed controller is less than 2×10^{-4} after 50 seconds, better than the results with PD and RFTFT controller, where the magnitude of attitude with RFTFT controller which will take more than 80 seconds to be less than 4×10^{-4}, and the magnitude of attitude with PD controller is 6×10^{-3} after the system is stable, much larger than the proposed controller. Also, in Fig. 5, the magnitude of angular velocity with proposed controller is less than 1×10^{-3} rad/s after 50 s, while angular velocity of the PD and RFTFT controller take more time to convergence to the neighborhood of zero. Besides, it can also be observed that the system overshoot with proposed controller is much less than PD and RFTFT controller. Fig. 8 and 9 show that the observer states are asymptotically stable and the estimation errors of the lumped disturbance convergence to a small neighborhood of zero. This means that inertia uncertainties, external disturbance and measurement uncertainties have been rejected well by proposed controller. As for the control torque and the acceleration angular velocity, it can be

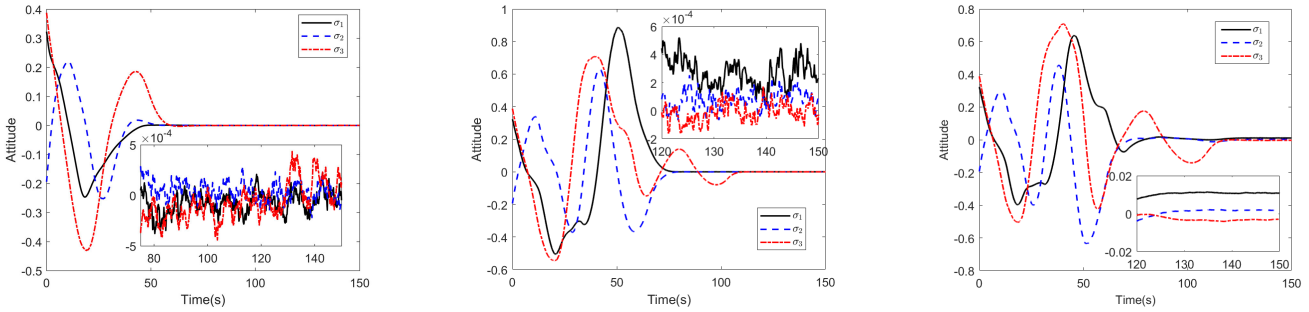

(a) Proposed controller (b) RFTFT controller (c) PD controller

FIGURE 10. Time history of attitude under tough condition.

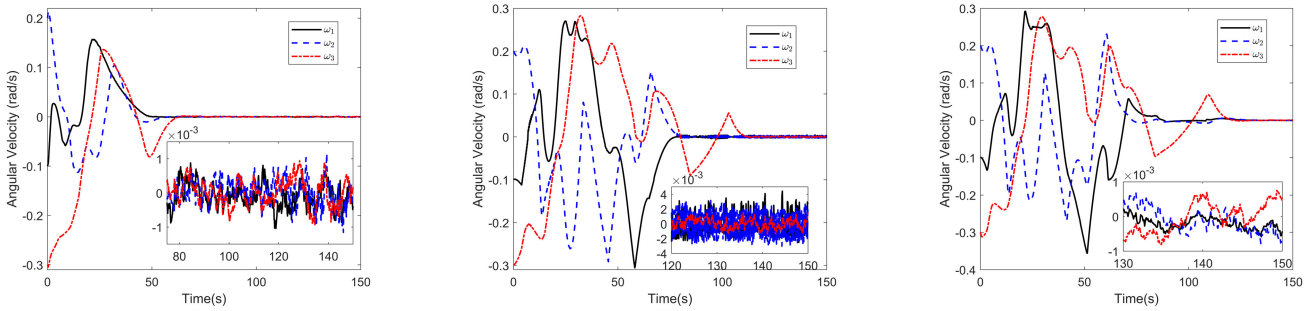

(a) Proposed controller (b) RFTFT controller (c) PD controller

FIGURE 11. Time history of angular velocity under tough condition.

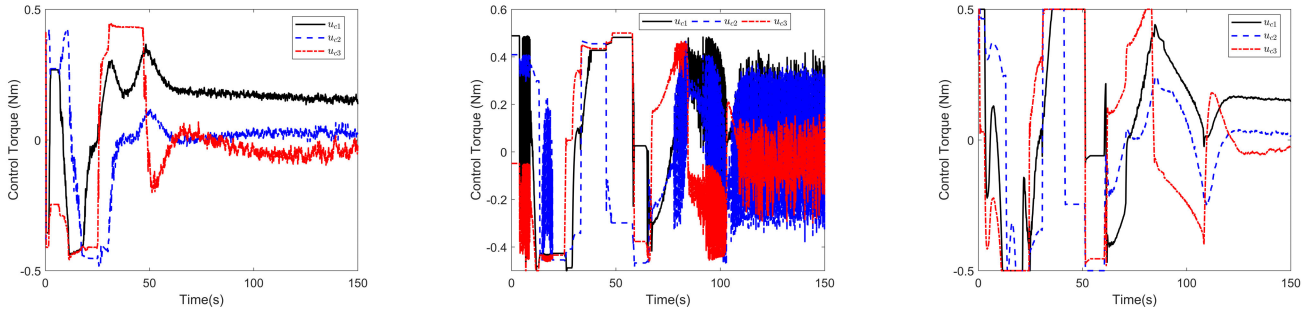

(a) Proposed controller (b) RFTFT controller (c) PD controller

FIGURE 12. Time history of control torque under tough condition.

seen that they are all constrained in the prescribed asymmetric limitations in Fig. 6 and Fig. 7, and the chatting phenomena has been obviously suppressed comparing to RFTFT controller. And moreover, the average value of the control torque and the angular acceleration velocity are listed in Table 2, where less control torque and acceleration angular velocity is needed to maintain the state in small neighborhood of zero of the proposed controller comparing to PD and RFTFT controller. In short, the proposed dynamic surface attitude stabilization controller with robust LMI-based control allocation method has better system performance and cost less control torque and actuator force than PD and RFTFT controller with psuedo-inverse control allocation method.

TABLE 2. Control torque and angular acceleration velocity with different controller.

Controllers	$\frac{1}{T}\int_0^T \|\boldsymbol{u}_c\|_2$	$\frac{1}{T}\int_0^T \left\|\dot{\boldsymbol{\Omega}}_w\right\|_2$
Proposed controller	0.2435	6.4245
PD controller	0.4508	8.3916
RFTFT controller	0.4357	6.7760

To show the robustness performance of the proposed controller, rough conditions are considered in this simulation by using controller (36). Especially, we set the nominal inertia matrix is $\boldsymbol{J}_0 = 0.6\boldsymbol{J} = \text{diag}\{7.2, 8.4, 13.2\}(\text{kg}\cdot\text{m}^2)$, the control input torque are $u_{ci\,\max} = 0.5$ and $u_{ci\,\min} = -0.5$ Nm, and

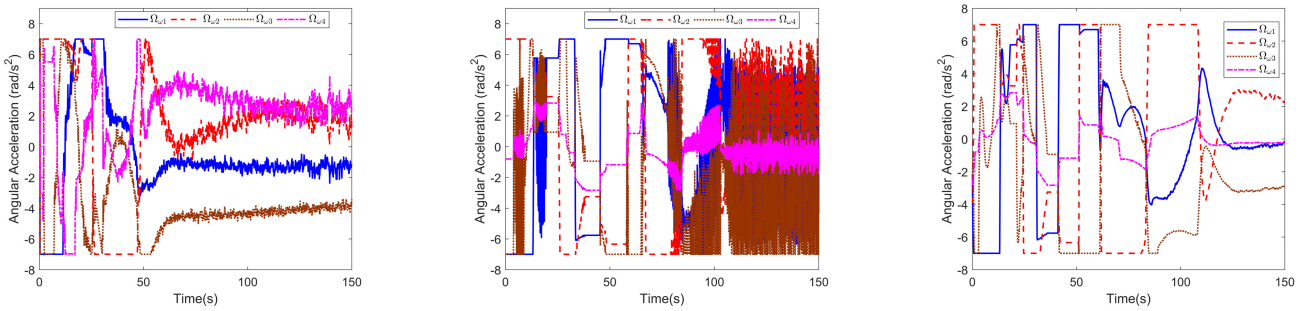

(a) Proposed controller (b) RFTFT controller (c) PD controller

FIGURE 13. Time history of angular acceleration of reaction wheels under tough condition.

TABLE 3. Control torque and angular acceleration velocity with different controller under tough condition.

Controllers	$\frac{1}{T}\int_0^T \|\boldsymbol{u}_c\|_2$	$\frac{1}{T}\int_0^T \|\dot{\boldsymbol{\Omega}}_w\|_2$
Proposed controller	0.2435	7.3968
PD controller	0.5258	9.0306
RFTFT controller	0.4634	8.0384

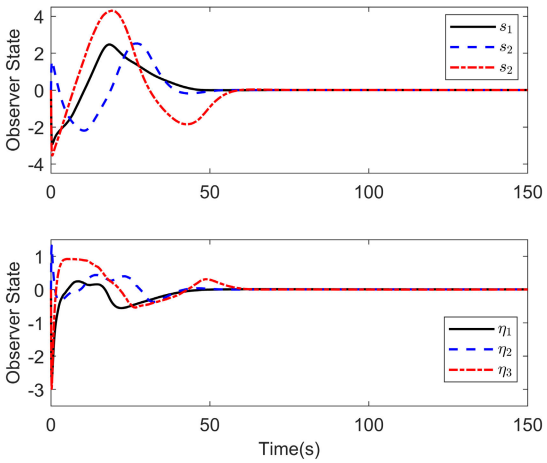

FIGURE 14. Time response of states of two disturbance observers under tough condition.

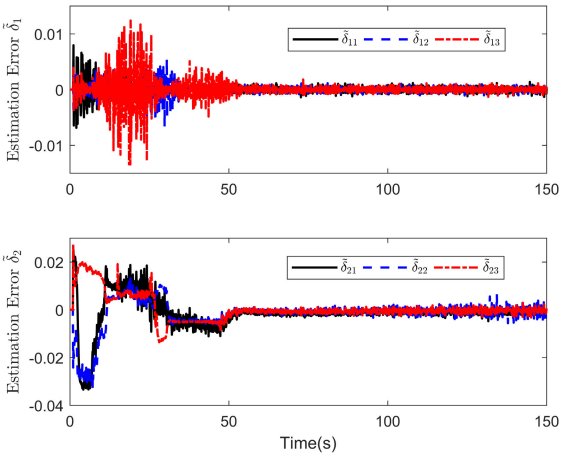

FIGURE 15. Time response of two estimation errors under tough condition.

the external disturbance model is $10\boldsymbol{d}$ and the measurement errors are the same form as (60). Then the simulation results are shown in Fig. 10-15. Fig. 10 presents the time history of the attitude trajectories under tough condition. Fig. 11 presents the time history of the angular velocity trajectories under tough condition. Fig. 12 presents the time history of control torque under tough condition. Fig. 13 presents the time history of angular acceleration of reaction wheels under tough condition. Fig. 14 presents the time history of states of two disturbance observers in proposed controller under tough condition. Fig. 15 presents the time history of two estimation errors in proposed controller under tough condition.

In view of the results in Fig. 10 and Fig. 11, we can see that the attitude and angular velocity with the proposed controller converge to small neighborhoods of zero in 75 seconds, while PD controller and RFTFT controller take 120 seconds, much longer than the proposed controller. And the magnitude of the attitude with proposed controller is less than 5×10^{-4} when system is stable, while PD controller is about 0.015 and RFTFT controller near 6×10^{-4} both larger than the proposed one. From Fig. 12 and 13, all the control torque and angular acceleration velocity are constrained in the limitation, and the chatting phenomenon is also effectively suppressed comparing to RFTFT method. Furthermore, the average value of the control torque and the angular acceleration velocity in this case are listed in Table 3. It can be seen that although more control torque and actuator force are needed in the tough condition, but the proposed method still costs less comparing to the other two control scheme. Fig. 14 and 15 show that observer states can convergence to a neighborhood of zero in finite time, and the estimation errors are bounded even under tough condition. In short, we can conclude that the closed-loop system is still stable with acceptable and better response performance in spite of rough conditions comparing to the other control scheme.

B. SUPERIORITY OF THE ROBUST LMI-BASED CONTROL ALLOCATION METHOD

In this subsection, the superiority of the robust LMI-based control allocation method is demonstrated. Considering that

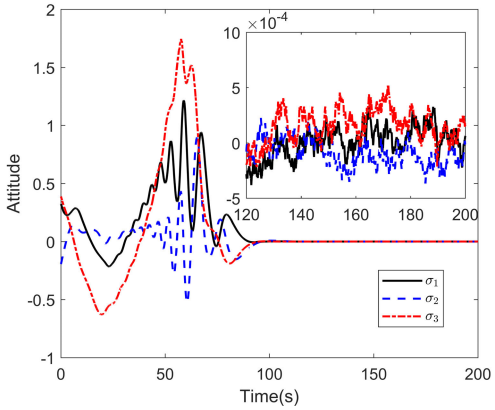

(a) Under robust LMI-based control allocation

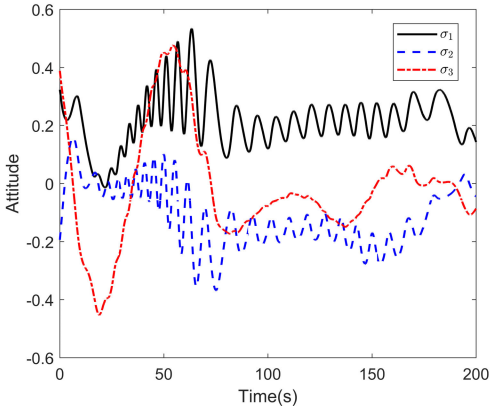

(b) Under psuedo-inverse control allocation

FIGURE 16. Time history of attitude with proposed controller under different control allocation method.

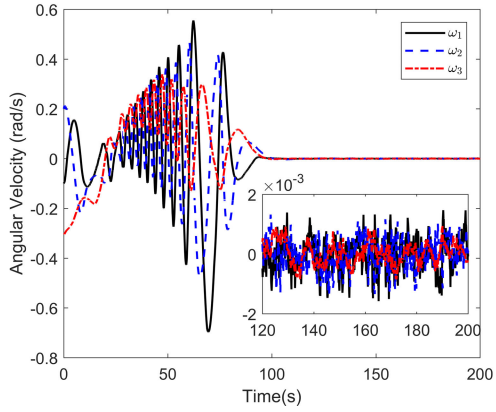

(a) Under robust LMI-based control allocation

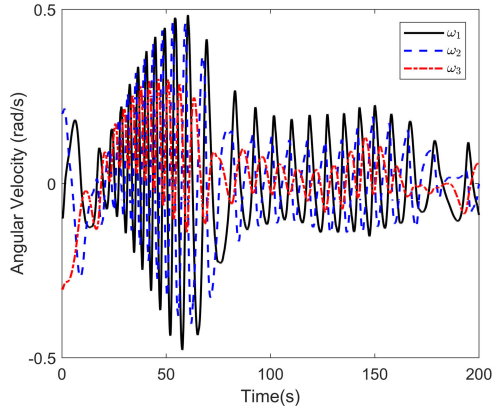

(b) Under psuedo-inverse control allocation

FIGURE 17. Time history of angular velocity with proposed controller under different control allocation method.

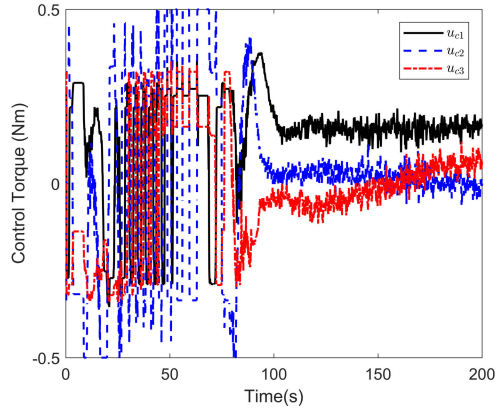

(a) Under robust LMI-based control allocation

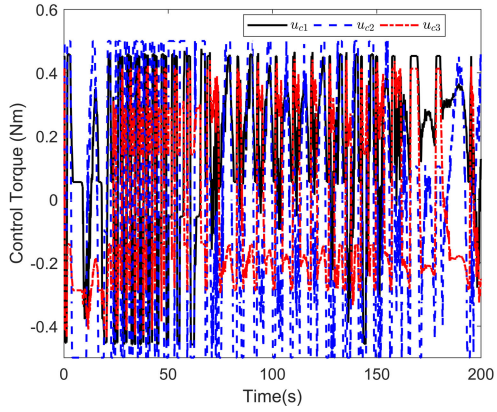

(b) Under psuedo-inverse control allocation

FIGURE 18. Time history of control torque with proposed controller under different control allocation method.

the control system is suffering a more serious condition, where the measurement error $\Delta \boldsymbol{r}_c$ satisfying $|\ \Delta r_{ci}\ | \leq 0.65$ m $(i = 1, 2, 3)$ and the other condition are same to the above tough condition. The simulation results are shown in Fig. 16-19. Fig. 16 presents the time history of the attitude trajectories in different control allocation methods. Fig. 17 presents the time history of the angular velocity trajectories in different control allocation methods. Fig. 18 presents the

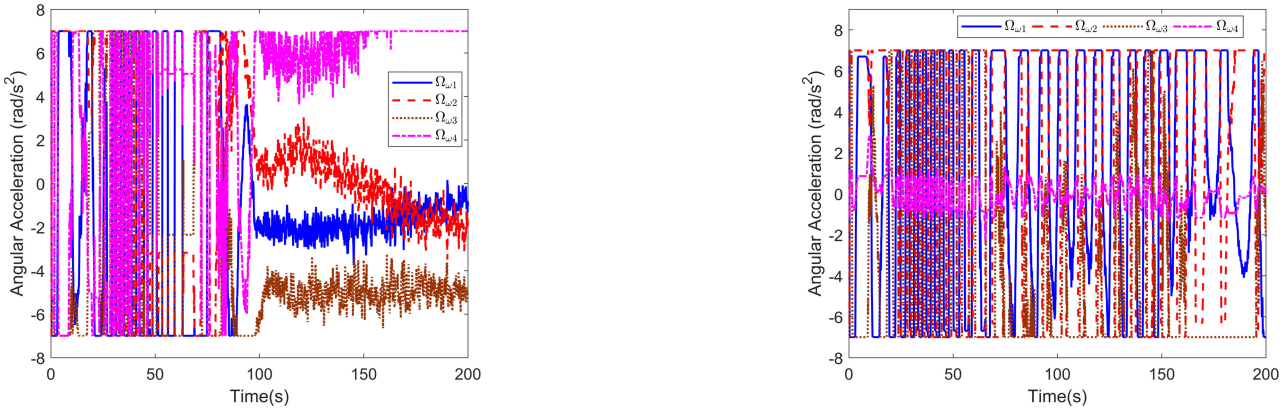

(a) Under robust LMI-based control allocation

(b) Under psuedo-inverse control allocation

FIGURE 19. Time history of angular acceleration of reaction wheels with proposed controller under different control allocation method.

time history of control torque in different control allocation methods. Fig 19 presents the time history of angular acceleration of reaction wheels.

In view of the results in Fig. 16-17, the attitude and angular velocity by proposed controller with robust LMI-based control allocation method is still stable, though more time is needed to convergence to the neighborhood of zero. However, the closed-loop states by proposed controller with psuedo-inverse control allocation method is diverging, i.e. the stability of the closed-loop system can not be ensured. Certainly, though more control torque and angular acceleration velocity are need from Fig. 18 and Fig. 19, they are still constrained in the limitation by the proposed control scheme. Thus, the proposed robust LMI-based control allocation method can guarantee the system stability even under serious condition while pseudo-inverse can not, which indicates that the proposed control allocation method is necessary in the control scheme.

V. CONCLUSION

In this paper, a control scheme combining attitude control of combined spacecraft with reaction wheels subject to actuator saturation, actuator fault, measurement uncertainty, inertia uncertainty and external disturbance is established. The proposed robust control allocation scheme, which uses disturbance-observer-based dynamic surface method to design the virtual feedback control, and employs the robust LMI-based control allocation scheme to suitably distribute the total virtual control torque into the active reaction wheels, enables the overall closed-loop states ultimately converge to an adjustable small neighborhood of zero. Simulation results have been carried out to show the advantages and improvements over existing controllers. In the future work, the extension of the proposed approach to output feedback control of combined spacecraft will be investigated.

REFERENCES

[1] A. Flores-Abad, O. Ma, K. Pham, and S. Ulrich, "A review of space robotics technologies for on-orbit servicing," *Prog. Aerop. Sci.*, vol. 68, no. 8, pp. 1–26, 2014.

[2] P. Huang, M. Wang, Z. Meng, F. Zhang, and Z. Liu, "Attitude takeover control for post-capture of target spacecraft using space robot," *Aerosp. Sci. Technol.*, vol. 51, pp. 171–180, Apr. 2016.

[3] X. Huang and G. Duan, "Fault-tolerant attitude tracking control of combined spacecraft with reaction wheels under prescribed performance," *ISA Trans.*, to be published. doi: 10.1016/j.isatra.2019.08.041.

[4] A. H. J. de Ruiter, "Spacecraft attitude tracking with guaranteed performance bounds," *J. Guid., Control, Dyn.*, vol. 36, no. 4, pp. 1214–1221, Jul./Aug. 2013.

[5] A. H. J. de Ruiter, "Observer-based adaptive spacecraft attitude control with guaranteed performance bounds," *IEEE Trans. Autom. Control*, vol. 61, no. 10, pp. 3146–3151, Oct. 2016.

[6] L. Sun and Z. Zheng, "Disturbance-observer-based robust backstepping attitude stabilization of spacecraft under input saturation and measurement uncertainty," *IEEE Trans. Ind. Electron.*, vol. 64, no. 10, pp. 7994–8002, Oct. 2017.

[7] L. Sun and Z. Zheng, "Saturated adaptive hierarchical fuzzy attitude-tracking control of rigid spacecraft with modeling and measurement uncertainties," *IEEE Trans. Ind. Electron.*, vol. 66, no. 5, pp. 3742–3751, May 2019.

[8] W. C. Durham, "Constrained control allocation," *J. Guid., Control, Dyn.*, vol. 16, no. 4, pp. 717–725, 1993.

[9] X. Hang and G. Duan, "A developed constrained control allocation approach based on pseudo inverse," in *Proc. Chin. Autom. Congr. (CAC)*, Oct. 2017, pp. 195–200.

[10] X. Huang and G. Duan, "Attitude control and structure robust control allocation for combined spacecraft," *Control Theory Appl.*, vol. 35, no. 10, pp. 1447–1457, 2018.

[11] O. Härkegård, "Dynamic control allocation using constrained quadratic programming," *J. Guid. Control Dyn.*, vol. 27, no. 6, pp. 1028–1034, 2004.

[12] X. Huang and G.-R. Duan, "Dynamic infinity-norm constrained control allocation for attitude tracking control of overactuated combined spacecraft," *IET Control Theory Appl.*, vol. 13, no. 11, pp. 1692–1703, Jul. 2019.

[13] Q. Hu, B. Li, and A. Zhang, "Robust finite-time control allocation in spacecraft attitude stabilization under actuator misalignment," *Nonlinear Dyn.*, vol. 73, nos. 1–2, pp. 53–71, 2013.

[14] Q. Shen, D. Wang, S. Zhu, and E. Poh, "Postcapture robust nonlinear control for tethered space robot with constraints on actuator and velocity of space tether," *IEEE Trans. Contrl Syst. Technol.*, vol. 25, no. 3, pp. 1068–1075, 2017.

[15] J. Luo, C. Wei, H. Dai, Z. Yin, X. Wei, and J. Yuan, "Robust inertia-free attitude takeover control of postcapture combined spacecraft with guaranteed prescribed performance," *ISA Trans.*, vol. 74, pp. 28–44, Mar. 2018.

[16] P. Huang, D. Wang, Z. Meng, F. Zhang, and J. Guo, "Adaptive postcapture backstepping control for tumbling tethered space robot–target combination," *J. Guid., Control, Dyn.*, vol. 39, no. 1, pp. 150–156, 2015.

[17] P. Huang, D. Wang, F. Zhang, Z. Meng, and Z. Liu, "Postcapture robust nonlinear control for tethered space robot with constraints on actuator and velocity of space tether," *Int. J. Robust. Nonlinear Control*, vol. 27, no. 16, pp. 2824–2841, Nov. 2017.

[18] S. Cao and Y. Zhao, "Anti-disturbance fault-tolerant attitude control for satellites subject to multiple disturbances and actuator saturation," *Nonlinear Dyn.*, vol. 89, no. 4, pp. 2657–2667, 2017.
[19] B. Xiao, Q. Hu, and Y. Zhang, "Adaptive sliding mode fault tolerant attitude tracking control for flexible spacecraft under actuator saturation," *IEEE Trans. Control Syst. Technol.*, vol. 20, no. 6, pp. 1605–1612, Nov. 2012.
[20] H.-T. Chen, S.-M. Song, and Z.-B. Zhu, "Robust finite-time attitude tracking control of rigid spacecraft under actuator saturation," *Int. J. Control Autom. Syst.*, vol. 16, no. 1, pp. 1–15, Feb. 2018.
[21] B. Zhou, H. Gao, Z. Lin, and G.-R. Duan, "Stabilization of linear systems with distributed input delay and input saturation," *Automatica*, vol. 48, no. 5, pp. 712–724, 2012.
[22] Z. Gao, Z. Zhou, M. S. Qian, and J. Lin, "Active fault tolerant control scheme for satellite attitude system subject to actuator time-varying faults," *IET Control Theory Appl.*, vol. 12, no. 3, pp. 405–412, Feb. 2018.
[23] D. Ran, X. Chen, A. de Ruiter, and B. Xiao, "Adaptive extended-state observer-based fault tolerant attitude control for spacecraft with reaction wheels," *Acta Astronautica*, vol. 145, pp. 501–514, Apr. 2018.
[24] Q. Li, L. Yin, H. Wang, X. Cao, and J. Cui, "Adaptive prescribed performance fault estimation and accommodation for a class of stochastic nonlinear systems," *IEEE Access*, vol. 7, pp. 14139–14149, 2019.
[25] Y. Miao, F. Wang, and M. Liu, "Anti-disturbance backstepping attitude control for rigid-flexible coupling spacecraft," *IEEE Access*, vol. 6, pp. 50729–50736, 2018.
[26] T. He and Z. Wu, "Extended disturbance observer with measurement noise reduction for spacecraft attitude stabilization," *IEEE Access*, vol. 7, pp. 66137–66147, 2019.
[27] D. Zhou and B. Xu, "Adaptive dynamic surface guidance law with input saturation constraint and autopilot dynamics," *J. Guid. Control Dyn.*, vol. 39, no. 5, pp. 1–8, 2016.
[28] P. Huang, M. Wang, Z. Meng, F. Zhang, Z. Liu, and H. Chang, "Reconfigurable spacecraft attitude takeover control in post-capture of target by space manipulators," *J. Franklin Inst.*, vol. 353, no. 9, pp. 1985–2008, Jun. 2016.
[29] A. H. de Ruiter, C. Damaren, and J. R. Forbes, *Spacecraft Dynamics and Control: An Introduction*. Hoboken, NJ, USA: Wiley, 2013.
[30] P. Singla, K. Subbarao, and J. L. Junkins, "Adaptive output feedback control for spacecraft rendezvous and docking under measurement uncertainty," *J. Guid., Control, Dyn.*, vol. 29, no. 4, pp. 892–902, Jul./Aug. 2006.
[31] M. Chen, B. B. Ren, Q. Wu, and C. Jiang, "Anti-disturbance control of hypersonic flight vehicles with input saturation using disturbance observer," *Sci. China Inf. Sci.*, vol. 58, no. 7, pp. 1–12, 2015.
[32] L. Guo and W.-H. Chen, "Disturbance attenuation and rejection for systems with nonlinearity via DOBC approach," *Int. J. Robust Nonlinear Control*, vol. 15, no. 3, pp. 109–125, 2005.
[33] G.-R. Duan and H.-H. Yu, *LMIs in Control Systems: Analysis, Design and Applications*. Boca Raton, FL, USA: CRC Press, 2013.
[34] J. Zhang, Q. Hu, and D. Wang, "Bounded finite-time attitude tracking control for rigid spacecraft via output feedback," *Aerosp. Sci. Technol.*, vol. 64, pp. 75–84, May 2017.
[35] J. T.-Y. Wen and K. Kreutz-Delgado, "The attitude control problem," *IEEE Trans. Autom. Control*, vol. 36, no. 10, pp. 1148–1162, Oct. 1991.
[36] Q. Hu, X. Huo, B. Xiao, and Z. Zhang, "Robust finite-time control for spacecraft attitude stabilization under actuator fault," *Proc. Inst. Mech. Eng. I, J. Syst. Control Eng.*, vol. 226, no. 3, pp. 416–428, Mar. 2012.

XIU-WEI HUANG received the B.E. degree in information and computing science and M.E. degree in control science and technology from the Harbin Institute of Technology, Harbin, China, in 2013 and 2015, respectively, where she is currently pursuing the Ph.D. degree in control science and technology. Her research interests include attitude control and control allocation of combined spacecraft.

GUANG-REN DUAN was born in Heilongjiang, China, in April 5, 1962. He received the B.Sc. degree in applied mathematics and the M.Sc. and Ph.D. degrees in control systems theory from the Harbin Institute of Technology.

From 1989 to 1991, he was a Postdoctoral Researcher with the Harbin Institute of Technology, Harbin, China, where he became a Professor of control systems theory, in 1991. He visited the University of Hull, U.K., and the University of Sheffield, U.K., from December 1996 to October 1998. He was a Lecturer with the Queen's University of Belfast, U.K., from October 1998 to October 2002. Since August 2000, he has been elected Specially Employed Professor with the Harbin Institute of Technology, sponsored by the Cheung Kong Scholars Program of the Chinese Government, where he is currently the Director of the Center for Control Theory and Guidance Technology. He is the author or coauthor of four books and more than 200 SCI indexed publications. Particularly, he has published a book, as the sole author, entitled *Analysis and Design of Descriptor Linear Systems* (NewYork: Springer, 2010). He has published more than 30 articles in IEEE Transactions. He has taught quite a few courses at the Harbin Institute of Technology and Queen's University of Belfast. Particularly, he has lectured the graduate course Introduction to Linear Matrix Inequalities in Control Systems Analysis and Design at the Harbin Institute of Technology, in the Fall semester from 2004 to 2005, and in the Spring semester from 2006 to 2011. His main research interests include parametric robust control systems design, linear matrix inequality-based control systems analysis and design, descriptor systems, flight control, and magnetic bearing control.